Charge-flow coupling in nanoscale water films in sphere-plane geometry

Marcela Rodríguez Matus

université de BORDEAUX

THÈSE PRÉSENTÉE

POUR OBTENIR LE GRADE DE

DOCTEUR
DE L'UNIVERSITÉ DE BORDEAUX

ECOLE DOCTORALE SCIENCES PHYSIQUES ET DE L'INGÉNIEUR

LASERS, MATIÈRE ET NANOSCIENCES

Par **Marcela RODRÍGUEZ MATUS**

Couplage charge-flux dans les films d'eau nanométriques en géométrie sphère-plan

Sous la direction de : **Alois WÜRGER**

Soutenue le 30 septembre 2021

Membres du jury :

M. Manoel MANGHI	Maître de conférences	Université Toulouse III	Rapporteur
M. Benjamin CROSS	Maître de conférences	Université Grenoble Alpes	Rapporteur
M. Frank CICHOS	Professeur	Universität Leipzig	Examinateur
M. Carlos DRUMMOND	Directeur de recherche	Université de Bordeaux	Examinateur
M. Abdelhamid MAALI	Directeur de recherche	Université de Bordeaux	Examinateur
M. Alois WÜRGER	Professeur	Université de Bordeaux	Directeur de thèse

Couplage charge-flux dans les films d'eau nanométriques en géométrie sphère-plan

Résumé : Les propriétés des électrolytes en contact avec une surface solide chargée sont un sujet d'intérêt depuis longtemps. Les progrès récents dans les études expérimentales et théoriques ont montré que l'écoulement liquide à l'échelle micro et nanométrique se comporte différemment de celui à l'échelle macroscopique. Lorsque les dimensions sont réduites, les propriétés de surface sont prédominantes pour le comportement de l'écoulement au contact de la surface. Pour une épaisseur encore plus petite, lorsque le fluide subit un confinement élevé, non seulement les propriétés physico-chimiques des surfaces de confinement sont importantes, mais leur comportement élastique doit également être pris en compte.

Cette thèse présente une étude théorique des propriétés des électrolytes confinés et de la mécanique de la double couche électrique dans une géométrie sphère-plan, où la sphère est montée sur un système cantilever qui oscille près d'une paroi solide. Nous dérivons les interactions électrocinétiques via le couplage du courant électrique et du flux de Poiseuille. Les flux de volume et de charge sont fermés par la loi de Gauss et une équation d'advection-diffusion pour les ions.

Nous avons obtenu la force électrovisqueuse, sans appliquer l'approximation de linéarisation, utilisée dans les travaux précédents. Ce travail fournit un bref rappel de la théorie de Poisson-Boltzmann et de la force répulsive statique. Ensuite, nous développons l'appareil formel pour le couplage charge-flux, nous dérivons le coefficient de traînée électrovisqueuse, et nous comparons diverses approximations analytiques avec le calcul numérique. Nous faisons une brève étude de la réponse visco-élastique, en fonction du produit de la fréquence d'entraînement et du temps de relaxation. Enfin, nous comparons les effets de la prise en compte d'une charge constante ou d'un potentiel de surface constant et nous confrontons les mesures dynamiques d'AFM à nos résultats théoriques.
Mots-clés : Microfluidique, Interfaces fluides, Couplage charge-flux

---

Charge-flow coupling in nanoscale water films in sphere-plane geometry

Abstract: The properties of electrolytes in contact with a charged solid surface have been a matter of interest for a long time. Recent progress in experimental and theoretical studies have shown that the liquid flow at micro and nanoscale behave differently from that at the macroscale. When the dimensions are reduced, the surface properties are predominant for the flow behaviour at contact with the surface. For an even smaller thickness when the fluid experiences a high confinement, not only the physico-chemical of the confining surfaces are important, their elastic behaviour should also be taken into account.

This thesis presents a theoretical study of the properties of confined electrolytes and mechanics of electric double layer in a sphere-plane geometry, where the sphere is mounted on a cantilever system that oscillates close to a solid wall. We derive the electrokinetic interactions via the coupling of electric current and Poiseuille flow. The volume and charge flows are closed by Gauss' law and an advection-diffusion equation for the ions.

We obtained the electroviscous force, without applying the linearization approximation, used in previous work. This work provides a brief reminder of Poisson-Boltzmann theory and the static repulsive force. Then we develop the formal apparatus for charge-flow coupling, derive the electroviscous drag coefficient, and compare various analytical approximations with the numerical computation. We make a short study of the visco-elastic response, as a function of the product of the driving frequency and the relaxation time. Finally, we compare the effects of considering a constant charge or a constant surface potential and contrast dynamic-AFM measurements with our theoretical findings.
Keywords: Microfluidic, Fluid Interfaces, Charge-flow coupling

---

Laboratoire Ondes et Matière d'Aquitaine (LOMA)
UMR 5798 Université de Bordeaux, 33405 TALENCE CEDEX, France.

To my parents and sisters

Acknowledgements

This dissertation is the result of four years of work carried at LOMA from the Université de Bordeaux. During these time, many people have directly or indirectly contributed to the realization of this dissertation, whom I would like to thank.

First and foremost, I would like to thank my thesis advisor: Alois Würger. Thank you for welcoming me to your group. I can not be as grateful as with you for giving me the opportunity to live this wonderful experience. Thank you for helping me in an endless list of things that made my PhD possible. I am particularly grateful for the constant support and patience. And of course for your great academic influence. Many thanks for showing me how to become a researcher.

I also thank all the members of my jury, Manoel Manghi, Benjamin Cross, Frank Cichos, Carlos Drummond and Abdelhamid Maali for the keen interest they have shown in reviewing this thesis work and their valuable feedback.

Thank you as well to Zouhir, Thibaut and Zaicheng for the exchange of scientific ideas that contributed to the development of this project, and all the members of the community in LOMA for making my PhD more enjoyable and full of good memories.

I thank the CONACyT for the financial support.

Last but not least, I thank all my family and friends from the bottom of my heart, you are the greatest motivator.

Abstract

The properties of electrolytes in contact with a charged solid surface have been a matter of interest for a long time. Recent progress in experimental and theoretical studies have shown that the liquid flow at micro and nanoscale behave differently from that at the macroscale. When the dimensions are reduced, the surface properties are predominant for the flow behaviour at contact with the surface. For an even smaller thickness when the fluid experiences a high confinement, not only the physico-chemical of the confining surfaces are important, their elastic behaviour should also be taken into account.

This thesis presents a theoretical study of the visco-elastic response of confined electrolytes and mechanics of electric double layer in a sphere-plane geometry, where the sphere is mounted on a cantilever system that oscillates close to a solid wall. We derive the electrokinetic interactions via the coupling of electric current and Poiseuille flow, by applying Poisson-Boltzmann mean-field theory and coupled linear relations for charge and hydrodynamic flows, including electro-osmosis and charge advection. With respect to the unperturbed Poiseuille flow, we define an electroviscous coupling parameter ξ, which turns out to be maximum where the film thickness h_0 is comparable to the screening length λ.

Our theory provides a quantitative description for the electroviscous drag coefficient and the electrostatic repulsion as a function of the film thickness, with the surface charge density as the only free parameter. We obtained the electroviscous force, with and without applying the linearization approximation, used in previous work. And evaluate the importance of charge regulation, that shows relevance only in small distances.

This work provides a brief reminder of Poisson-Boltzmann theory and the static repulsive force. Then we develop the formal apparatus for charge-flow coupling, derive the electroviscous drag coefficient, and compare various analytical approximations with the numerical computation. We make a short study of the visco-elastic response, as a function of the product of the driving frequency and the relaxation time. Finally, we compare the effects of considering a constant charge or a constant surface potential and contrast dynamic-AFM measurements with our theoretical findings.

Contents

Chapter 1

Introduction

For more than a century, the properties of electrolytes in contact with a charged solid surface have been of interest, motivated by their effects in biological and colloidal systems [1]. In fact, the coupling between electrostatic effects induced by the charged surface and hydrodynamic transport effects allows the manipulation of colloid solutions. However, these electrokinetic phenomena are not limited to the study of colloids but occur whenever a charged solid-liquid interface is involved. For example charged membranes separating dilute aqueous salt solutions. In 1968 R. J. Gross and J. F. Osterle [2] realised that there was not a membrane permeation general theory has been established. so they conducted a theoretical study of steady-state electrodynamics flow with adsorbed electrical charges on the wall.

In addition, Bike and Prive [3] focused on the study of the sliding and squeezing motion of two charged bodies immersed in an electrolyte solution. Observing that, for two bodies separated by a minimum distance, a streaming potential given by the motion of the surfaces creates electrical stress that contributes to a force that is felt by the two bodies. These electrokinetic force does not rely on the fluid's viscosity but depends on the non-equilibrium properties of the electric double layer, which exceed by far the electrostatic repulsion and therefore acts to keep the interacting bodies apart [4].

Since then, many attempts to find a correction to Bike and Prive's approach have been

studied. For instance, by introducing nonlinear electric effects, Chun and Ladd [5] found that the repercussions in the lifting force are significant. It was shown that when the ion diffusivities are considerably different, the force can be reduced by one order of magnitude.

In addition, it has been observed by Manor et al, that when the surfaces approach, the velocity of the approximation will determine the type of forces that will dominate in the system, for instance, at low scan rates ($<=1\mu$m/s), the interaction will be dictated by equilibrium forces and be independent of hydrodynamic boundary conditions. Which is not the case when the velocity increases as dynamic effects dominate [6].

The electrostatic repulsion creates an increment in the viscosity in the trapped electrolyte, that is associated to properties of the solid surfaces and is proportional to the surface charge density [7]. For its part, the ion concentration plays a big role on the electro-kinetic phenomena, on the one hand, in the dilute limit a strong electrical conductance is measured in narrow channels, where for low concentrations it shows higher values that those expected for bulk [8]. On the other hand, where strong screening effects emerge at high concentration [9]

In addition, the electroviscous effects are strongly dependent on the electrical potential at the slipping plane, as a repercussion of the counter-ion conductivity of the electric double layer [10].

Nanoscale flows of electrolytes in confined geometry are of primary importance for active matter, energy storage devices, harvesting of waste energy, de-salinization, and actuation and signal detection in micromechanical systems [11, 12]. Surface properties are predominant for flow behaviour and ionic transport in these systems. Solid surfaces in contact with electrolyte solutions are mostly charged. The coupling of the diffuse layer of counter-ions to liquid flow is at the origin of various electro-kinetic and visco-electric effects, leading to novel and original applications.

Electrophoresis through nano-pores is a most promising technique for the miniaturization of simple circuits, considering that it has been observed that nano-pores behave

like nano-fluidic diodes, this by permitting the flow in only one direction of the ionic flow [13, 14]. As a consequence it is a very useful technique as well for DNA sequencing, seeing that it offers the possibility to read information from single molecules of DNA[15, 16]. Another original application is the the assembly of active materials, by applying a a.c. electric field, charge-induced electro-osmosis controls the mobility of the particles as well as the colloidal interactions [17], observing different structures as a function of the electric field.

Complex electro-hydro-mechanical couplings have been specifically investigated in highly concentrated electrolytes known as ionic liquids, where by effect of the charges confined in nanoscale distances, the restrained liquid experiments structural alterations. By generating an order in between layers, under the influence of an electric field solidification and melting is predicted [18]. Experimentally, by measuring the friction force experimented between two solid surfaces that trap an ionic liquid, it has been observed that a layered ion structure is formed, conferring a quantized friction behaviour [19].

In aqueous medium, the electrostatic force should be considered, taking into account that many surfaces are charged while in water. This charge can be generated from two different phenomena. The dissociation of surface groups or by the absorption of ions into the surface. Due to the charges on the surface, an electric field will be generated, this electric field will decrease exponentially with the distance from the surface.[20, 21]

The first layer consists of the ionisation of the surface of the object, acquiring a surface charge density and is caused by chemical interactions; the degree of the surface charge density depends on the counterions on the surface and the free ions inside the fluid that it is immersed [22].

On the other hand, inside the fluid, there are free ions that are moving in it due to pressure, electric or thermal effects and that as a result of Coulomb force, will be attracted to the surface of the object, electrically screening the layer on the object surface. This second layer is also known as diffuse layer since it is roughly associated with the object.

In many instances, the underlying electro-kinetic effects are coupled to a non-uniform pressure, such that the fluxes of both volume and charge are driven by the electric field and the pressure gradient. The volume flow consist of Poiseuille and electro-osmotic contributions, and the charge current is determined by the electrical conductivity and advection of the diffuse layer by the Poiseuille flow.

1.1 The Electric Double Layer

When an object is immerse in an aqueous system, this object could be a solid particle, a gas bubble, a liquid droplet or a porous body; the object may selectively adsorb one charge species. This phenomena have been highly studied for colloids, where electrical interaction in aqueous systems is greatly significant in the stability, aggregation and deposition of the particles. So when a particle is exposed to a fluid, a structure of ions appears on its surface causing an electrical double layer. This double layer refers to two parallel layers of charge surrounding the object.

The first layer corresponds to the surface charge generated either by adsorption of ions from an electrolyte solution due to chemical interactions, dissociation of the surface compound, or redistribution of the electron density. On the other hand the second layer is composed of ions attracted to the surface charge due to coulomb force, and thus these ions screen the first layer. This second layer is called diffuse layer because it is loosely attached to the object, since it is made of free ions that move in the fluid under the influence of electric attraction and thermal motion. In such manner, both the surface charge and the associated attracted ions compose the electrical double layer.

In other words a particle's surface charge is balanced by an equivalent number of oppositely charged counter-ions in the fluid.

The counterions in the solution are experimenting two interactions that counterbalance. The attraction towards the particle given by electrostatic forces and the effect of the thermal energy that diffuses them randomly throughout the solution [23]. These electric

forces and thermal motion keeps an balanced distribution of the ions in the solution, deriving in an equilibrium; where some of the excess counterions will get near to the surface and the rest will dilute as a function of the distance of the surface [24], as shown schematically in Figure 1.1 .

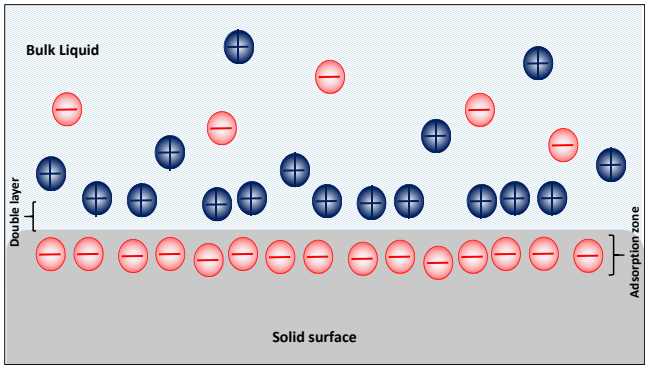

Figure 1.1: Graphic of the electrical double layer in aqueous solution at the interface with a negatively-charged surface of a solid. where the blue spheres represent the cations and the red spheres the anions. The increased number of cations closer to the surface that is negatively-charged forms the electric double layer.

As expected, the part of the solvent that is the closest to the particle will be mostly constituted by the counterions, this part of the fluid together with those charges that are strongly attached to the particle is what is called the **Stern layer**. This interaction is strong enough, that even if the particle moves in the medium, the Stern layer will move with it. However, the amount of counterions that are adsorbed into the surface of the particle tends to be smaller than the ions in the surface of the object, therefore the potential created at this distance will still be negative.

As one can see in Figure 1.2, around the Stern layer there is a covering of ions and counterions, that tends to be more charged of the second type, and it is known as **diffuse layer**. The ions in this layer are more mobile due to the thermal energy and can move from and towards the electrically neutral zone, where the concentration of ions and counterions are equal, so the medium can be seen as a continuum.

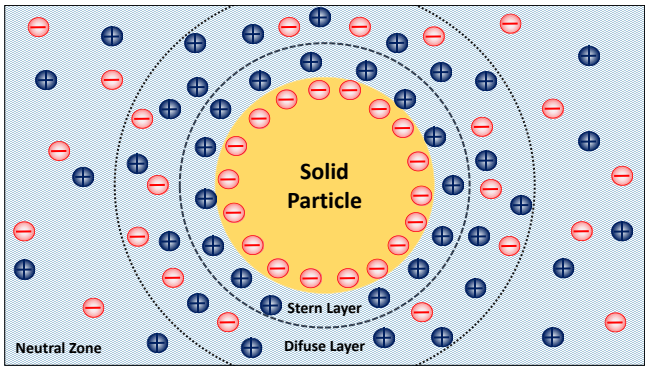

Figure 1.2: Graphic of a particle immerse in a fluid creating a disperse system. Adapted from [24]

The electrical double layer as the result of the variation of electric potential near a surface, has an influence on the behaviour of colloids and other surfaces in contact with solutions. This implies that the electrical potential in the fluid will depend greatly of it's exact position.

The difference in electric potential between the surface and the bulk area of the fluid where electrical neutrality is reached is known as the Nernst potential. It is to be expected that the Nernst potential is controlled by the ions at the surface of the particle that create an initial electrical potential. Then, the difference in the potential between the plane that divides the diffuse layer (slipping plane) and the neutral region is referred as the electrokintic or **zeta potential** ζ, this plane of shear separates the fixed from the mobile parts of the electrical double layer. As one can see from figure 1.3, the ζ potential decays exponentially from the Stern layer while reaching the neutral region.

It is the zeta potential that determines the repulsion between, similarly charged solid surfaces immerse in a fluid. It has been observed that depending on the characteristics of system under investigation, since the surface charge and the distribution of counterions near to the surface depends greatly on the nature and concentration of salt in the solution, if the zeta potential is reduced under a certain value, the attractive forces between particles due to van der Waals' force, overcome the forces of repulsion and the particles come together

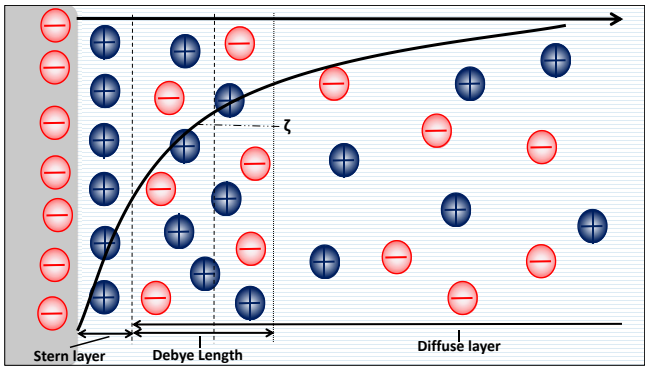

Figure 1.3: Relationship between Stern layer, Debye length and ζ potential. Adapted from [24]

[25] whereas they will be stable if the zeta potential value is larger.

To describe how the electric double layer is formed a two step process is suggested. It starts with the molecules in the fluid approach the surface, that initially is not charged and the atoms in the solution interact with the atoms on the surface of the object creating a electron cloud. This leads to the transfer of electrons towards the surface forming ions and charging the surface. Hereafter, the ions in the liquid will feel attracted approaching the particle's ions due to electrostatic interactions. Both electron transfer and ion transfer co-exist at liquid-solid interface [26, 27].

1.2 Electrokinetic effects

Once the double layer is formed, different effects occur from the behaviour of the liquid close to the interface. These effects known as electrokinetic phenomena generally refer to the tangential motion of liquids with respect to charged solid surfaces [28], the induced flux is created by an applied thermodynamic gradient and part of the double layer charge moves with the fluid.

These electrokinetic effects have important industrial and biological applications. They began to be studied as a characterization tool for colloids. But have been used as well to

manipulate particles and liquids in micro and nano scale and for energy conversion [29].

The main electrokinetic phenomena are [30]:

- **Electrophoresis**, the motion of particles in a suspension generated by an applied electric field.
- **Electro-Osmosis**, the flow of a liquid though a capillary when an electric field parallel to its axis is applied. This effect can be related to the electro-osmotic pressure, when applying an electric field a difference in pressure will rise if the there is not possible flow.
- **Electroviscous effect**, this is related to the increase of the viscous drag.

Electrophoresis

The most common electrokinetic method used to study colloid systems is electrophoresis. This method considers that the particles that are in the suspension will move under the effects of an applied electric field. The colloidal particles move with a constant velocity as a result of the balance between the applied electric field acting on the particles and the resistance felt by the particles created by the liquid. For particles' size large compared with the double layer thickness the velocity of the particles is proportional to the applied field, and allows to define the eletrophoretic mobility μ as

$$\mu = v/E = \varepsilon\zeta/\eta \tag{1.1}$$

Where v is the particle velocity and E the electric field.

In the case of hard particles without surface structures the electrophoretic mobility μ depends on the zeta potential ζ of the particle as a function of the viscosity of the solution η and using Smoluchowski electrophoresis theory [31].

With ε the dielectric constant of the dispersion medium, ε_0 is the permittivity of free space. This expression applies to particles in electrolyte solution that are large and not

too diluted. On the other hand, if the particles are smaller than the double electric layer both the drag force and the electric force acting on the particle will balance in static state condition, leading to an expression known as Hückel equation

$$\mu = 2\varepsilon\zeta/3\eta \tag{1.2}$$

Electrophoresis applied in media such as gel, is widely used to separate macro-molecules based on size and electrical charge as well as in DNA, RNA and protein analysis. The technique consist in applying a negative charge so proteins move towards a positive charge through a gel, allowing smaller molecules to move faster than larger ones. The human genome, for example, was obtained by capillary electrophoresis, by dividing the DNA in shorter pieces and the make them move in a gel until they separate. This technique has now attracted attention in biomedical analysis as an approach that can provide high efficiency so it is migrating towards the clinical diagnosis and forensics, developing microchip electrophoresis as a miniaturized form of conventional capillary electrophoresis [32].

The main advantages of using capillary electrophoresis are the higher separation efficacy and the small sample volume required. This makes it highly attractive for biological cases where monitoring body fluids with limited availability is required [33].

Electro-osmosis

Another well studied electrokinetic phenomena is the electro-osmotic flow, the motion of liquid induced by an applied potential along a capillary. Due to friction forces, the movement affects over the whole volume of the channel, because it takes place in ranges of time in the order of 10^{-4} to 10^{-2}s, as a result the whole volume of the liquid flows in the channel [34–36]. Figure 1.4 shows how due to electro-osmosis the fluid trapped in a capillarity is dragged in the same direction as the applied electric field.

Because electro-osmotic velocities are independent of conduit size, as long as the electrical double layer is much smaller than the length scale of the channel, electro-osmotic

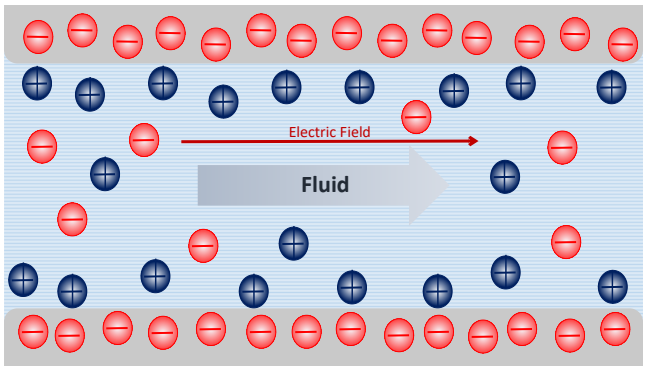

Figure 1.4: Diagram of electro-osmotic effect. Then electric field pushes the negatively charged surface in one direction and the diffuse layer in the other, since the solid surface is fixed only the liquid moves.

flow will have little effect on the diffuse layer. However if a voltage is applied between the two ends of a small channel, the ions of the double layer are moved by the influence of the electric field.

In contrast with the electrophoretic effect where the solid surface is that of a mobile particle, which starts moving itself when the liquid moves along its surface, the electro-osmotic flow causes the liquid to move as a whole with respect to the lab reference frame. The velocity profile in a channel due to electro-osmosis is zero at the wall but in a very short distance, which is approximately equal to the thickness of the diffuse layer, it reaches a constant value across the rest of canal.

Assuming that the fluid velocity is zero in at the shear plane $\Psi = \zeta$ and reaches a constant value when the potential $\Psi = 0$ and considering ϵ and η constant, the electro-osmotic velocity takes a very simple form

$$v_{eo} = \frac{E\epsilon\zeta}{\eta} \tag{1.3}$$

Considering that the force per unit length of a channel is proportional to the perimeter of the channel and the amount of fluid that will be moved is proportional to the cross section area, the electro-osmotic effect becomes significant in really narrow channels, for

example in microfluidic devices or porous media [37].

In the case of microfluidics, where elctrokinetics is relevant, the flows can be described by a continuous approach but special attention has to be given to surface effects and geometrical features. Microfluidic flows can be manipulated with different external fields: pressure, electric, magnetic etc. To employ electro-osmotic flow as a way to transport fluid by applying voltages along a channel has been widely applied in micro-fluidic devices since it has the advantage that in uniform channels the flow has a constant velocity over the channel cross-section and that electric and fluidic circuits can be integrated on the same microchip to build complex miniaturized devices without moving parts.

Electroviscous effects in capillaries due to a pressure gradient

An electric potential gradient induces a global velocity and thus a fluid flow rate Q. In classical macroscopic applications, the flows are induced by a pressure difference inducing a parabolic profile called Poiseuille profile. However, Poiseuille-induced flows are very sensitive to pressure drops, which become very important with decreasing channel size.

Just as an electric potential difference induces a flow, a ∇P pressure gradient can induce an electric current when double layers are involved: This phenomenon is called streaming current. A hydrodynamic flow carries away the ions present in the diffuse double layer. The excess of counter ions with respect to the co-ions, leads to a global flow of charges, this is the streaming current, that is related to a streaming potential.

At the interface between a solid and a flowing liquid, when the liquid flows through a channel under a pressure gradient ∇P, the generated streaming electric field is counter directed resulting in a retardation of the liquid flow manifests itself as an apparent enhanced fluid viscosity [38, 39].

In the case that we study, when the capillary is closed at one end, the charges accumulates, this accumulation of charge is responsible of creating an electric field [3, 5]. It has been found that this **electroviscous force** depends on the size of the ions present in the double layer [40, 41].

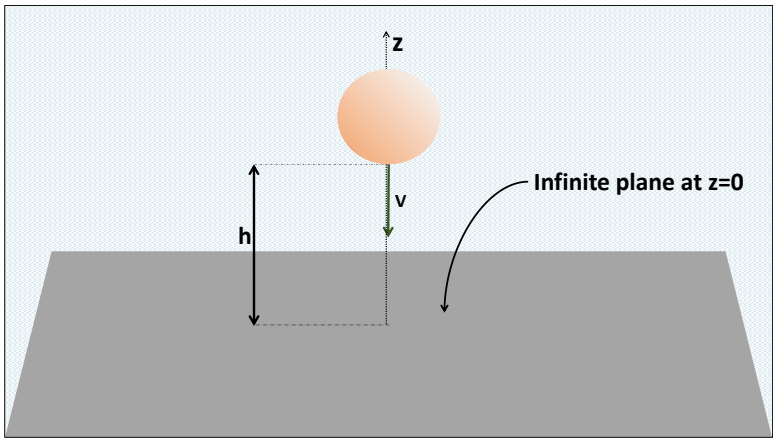

Figure 1.5: Schematic sketch.

1.3 AFM and SFA measurements

The resistance offered by a fluid, is called the drag force. It acts in a direction opposite to the object's motion. It is generated by the relative velocity between the solid object and the fluid. Whether the object or fluid is moving, drag occurs as long as there is a difference in their velocities. Drag force depends on the viscosity of the fluid, the upstream velocity, and the size, shape, and orientation of the body and because it is resistant to motion, drag tends to slow down the object.

Stokes law, for the resistance of a sphere ascending or descending in a fluid abstains the frictional force as [42]

$$F_0 = 6\pi\eta RV \tag{1.4}$$

considering a solid sphere of radius R that moves with constant velocity V immerse in a fluid of viscosity η (see figure 1.5), the solution for the drag force given in 1.4 is valid for the case when the distance $h >> R$. Still this well known relation applies only to fluid media that extend to infinity in all directions, while in most real situations, the fluid is limited by rigid or free walls. Therefore, the presence of those boundaries at a finite distance from the object require a correction to stokes formula [43].

One common way of studying flows near boundaries is to consider a sphere moving towards a flat surface. From a classical approach, it is assumed that there is no slip at the boundary between the liquid and the surface and by denoting ξ_c as the correction which must be applied the drag force takes the form

$$F_c = -\frac{6\pi\eta R^2 V}{h}(1+\xi_c) \tag{1.5}$$

where h corresponds to the distance between the bottom of the sphere and the surface [44]. Here $\xi_c \approx (1+\alpha R/h)$ with α a correction constant. Contrary to the system described in equation (1.4) is only valid when $h << R$.

During the last decades, several different techniques for measuring surface forces both in air and in liquids, allowing to estimate accurately from the macroscopic to the molecular scale. In the **surface force apparatus** (SFA) technique two smooth cylindrical curved surfaces whose cylindrical axes are positioned at 90° to each other are made to approach each other in a direction normal to the axes. One of the surfaces is mounted on a spring, which is deflected by the presences of the normal force. this technique measures the separation of the two surfaces h with interferometry and the changes in $h$is used to calculate the force being exerted between the surfaces [45, 46].

As typically the radius of the cylinders are larger that the separation between the surfaces h, the system can be represented as a one-dimensional capacitor where the separation between the surface can be considered constant along the cylinder.

A **atomic force microscope** (AFM) is a mechanical microscope, that obtains information of the studied surface by "touching" it with a mechanical probe, in other words, the AFM is a cantilever with a micro-fabricated tip that deflects when interacting with the sample surface. A big advantage is that this technique offers is that it is not restricted by the optical diffraction limit as in the case of light microscopes allowing a resolution down to a single atom and subatomic features on a surface. The most used method to detect the motion of an AFM is optical beam deflection. A laser beam is focused on a spot of the

cantilever and the angular deflection of the reflected beam is detected [44, 47–56].

AFM is also helpful to study surface interactions by means of force-distance curves, through the measuring of the forces between the probe and the sample as a function of their mutual separation. These forces can be as weak as pico-Newton, and are necessary to create van der Waals forces and to stretch and rupture biological molecules.

While AFM can be performed in vacuum and in air, where a constant force acts on the sample by touching the surface, it is not ideal in all cases, since it can move or damage the object. So to reduce the perturbation AFM in liquid medium was developed, reducing the contact time and therefore the disturbance of the sample. However, the measured deflection of the cantilever is not only generated by features on the studies surface, when the cantilever oscillates near the surface, the fluid squeeze out the region directly underneath the tip, resulting in an additional hydrodynamic force acting on the cantilever and opposing the motion [57]. In addition, when the tip of the cantilever is in the aqueous medium above a charged surface, it experiences electrostatic, van der Waals and hydration forces.

Even if the tip does not carry electric charges, if there is an electric field polarization at the interface of the surface and the electrolyte will produce electrostatic interactions, causing an osmotic pressure that repels the tip. So when the sample moves towards the tip, this forces repel the tip, and the cantilever bends away, therefore the distance that is measured is larger that the expected. Butt observed [21] that by modifying salt content in the fluid as well as the pH the electrostatic forces can be tuned, increasing or decreasing the value and becoming attractive for some values of pH depending on the characteristics of the tip and surface material.

This thesis focuses on the investigation of the dynamic properties of electric double layers in a confined geometry, where the inherent electro-kinetic effects couple to a non-uniform pressure.

To this end, we propose a theoretical model to quantify the visco-elastic and electro-dynamic response induced by non-equilibrium electric double layers, as a function of the

gap width and the driving frequency.

To answer this question, we will proceed with the following plan:

- Initially, we will present a brief overview of the equilibrium phenomena as well as the transport phenomena involved in electrolyte systems in the vicinity of electrolytes in the vicinity of charged surfaces.

- We will present in detail in chapter 2 the main features of the theoretical basis for our study, starting with the electrostatic potential obtained trough the Poisson-Boltzmann theory and the characterization of the effects observed in the capillarity, expressing it in a closed equation system for the volume and charge flow generated due to generalised forces.

- In chapter 3 we present different approaches to obtain the coupling of charge and flow for a confined fluid and the results for the drag coefficient. The definition of the coupling coefficient is given by the transport coefficients studied in chapter 2 and that can be calculated analytically if we consider a wide channel and narrow channel limits. In addition we obtain a general solution by taking a numerical approach and that gives a solution for the full range of distance. Additionally, we study the effects of different boundary conditions for the electrostatic potential.

- An analysis of time dependency is discussed in chapter 5. He we include the effects of the oscillation frequency in the system as well as the retardation time of the charges. We approach this problem via relaxation time approximation and series expansion.

- In chapter 6 we compare the results obtained for the electroviscous force with experimental data obtained via AFM force measurement and analyze the advantages of our model with the previous work presented in the literature.We get the general conclusions of this work in the chapter 7

⇀ Finally, in **??** we discuss possible approach to continue the presented work.

Chapter 2

Formal Apparatus

2.1 Poisson-Boltzmann theory

Electrostatic interactions constitute a key component in understanding interactions between charged bodies in ionic solutions. For example, the stability of colloidal particles dispersed in a solvent can be explained by considering the competition between repulsive electrostatic interactions and attractive Van der Waals interactions[23, 58–61].

As any charged object immersed in an ionic solution, the membrane attracts a cloud of opposite charges forming a diffusive 'electric double layer'. The exact distribution of the charges is given by the competition between the electrostatic interactions and the entropy of the ions in the solution which tends to disperse them. This diffusive electric double layer in turn influences the overall electrostatic interactions of the membrane with its environment as well as the 'internal' membrane properties.

The electrostatic interactions will have an structural effect when the thermal energy K_BT is in the order of the Couloumbic energy between two charged objects. This distance l_B is defined as the *Bjerrum length*

$$l_B = \frac{e^2}{4\pi\varepsilon k_B T} \tag{2.1}$$

where e is the elementary charge, ε is the relative dielectric constant of the medium. For

water at room temperature $T = 300$ K and $\varepsilon \approx 80$ so that $l_B \approx 0.7$ nm.

Whatever the origin of the surface charge, it must be balanced by an equal and opposite charge in the solution, with a surface potential ϕ and a surface charge density σ, it is possible to describe the distribution of charge and potential in the solution as a function of the distance of the surface. As a mean-field theory, Poisson-Boltzmann theory replaces all interactions to the body with an average interaction without loss of generality, and so it base on a number of simplifying assumptions:

i An infinite, flat and impenetrable interface.

ii The aqueous solution is a continuous media with a dielectric constant ε independent of the distance to the surface.

iii Only Coulomb interactions are considered between charged bodies.

iv The surface charge is assumed continuous and the mobile ions are modelled as point objects that are able to approach right up to the interface.

v Dipole interactions are neglected

vi Both the electrostatic potential $\phi(r)$ and the density profile $\rho(r)$ are mean-field continuous functions of the position r

These assumptions can be modified in more refined versions of the theory. Nonetheless, the rate of exchange of protons and other ions between the surface and the solution tends to be very rapid, thus, many surfaces can be assumed to have a uniform surface charge.

Consider an ionic solution with two ionic species having positive and negative charge densities $\rho = \rho_+ + \rho_-$, if we assume that the membrane is negatively charged and take the surface charge density as a negative constant, $\sigma < 0$.

There are two possible situations:

- No electrolyte is added to the water: Here the only ions in the solution are the counterions balancing exactly the charges within the charged surface due to charge

neutrality. since we are considering a continuum, the counterions in the solution are described by a charge distribution

$$\rho_{\pm} = ez_{\pm}n_{\pm} \tag{2.2}$$

Where $n_{\pm}$ is the number density of the counterions.

- The solution is in contact with an electrolyte reservoir of fixed concentration n_0: both co-ions and counterions are present in the solution. Under these condition the total charge density will be the addition of the two ionic densities

$$\rho = e(z_+n_+ + z_-n_-) \tag{2.3}$$

Here $z_+ > 0$ is the valency of the cations and $z_- < 0$ is the valency of the anions.

Here we resume known results on the 1D Poisson-Boltzmann problem, following closely Andelman's review [58, 59]

Since the ions in the fluid are considered in thermodynamic equilibrium and they can move, they adapt to the presence of electrostatic conditions, either a constant surface potential, a constant surface charge density, or due to releasing and recovering of surface protons, charge regulation. The relation between the electric potential ϕ and the charge distribution at all point inside the fluid is described by the Poisson equation considering the dielectric constant ϵ

$$\nabla^2\phi = -\frac{1}{\epsilon_w}\rho = -\frac{e}{\epsilon_w}(z_-n_- + z_+n_+) \tag{2.4}$$

When the system is in thermal equilibrium, in the solution, the charge density depends on the local distribution of ions and cations, all of them follow the Boltzmann distribution that is a function of the potential.

$$n_i = n_0 e^{-ez_i\phi/k_BT} \tag{2.5}$$

Where n_i is the number concentration of the ions i at a point where the potential is ϕ and n_0 is the reference density at $\phi \to 0$ (bulk solution). the exponential therm represents the electrical energy on an ion with a charge $-ez_i$ relative to its thermal energy k_BT If we combine the last two equations we find

$$\nabla^2\phi = -\frac{e}{\epsilon_w}\left(z_+ n_0 e^{-ez_+\phi/k_BTT} + z_- n_0 e^{-ez_-\phi/k_BTT}\right) \tag{2.6}$$

That is known as the **Poisson-Boltzmann** equation for the potential ϕ.

In the particular case, when the system is in contact with an infinite reservoir of electrolyte, one can find a solution of the form

$$\nabla^2\phi = \frac{2en_0}{\varepsilon}\sinh\frac{e\phi}{k_BT} \tag{2.7}$$

Where it is assumed that the electrolyte is monovalent ($z_\pm = \pm 1$ and $n_0 = n_-^0 = n_+^0$).

The simpler case to solve applying Poisson-Boltzmann theory is the 1D solution for a single surface that is in contact with a infinite half-space of an electrolyte. It consist of a planar surface that has a fixed surface charge density σ and the profile of counterions that form a diffuse layer in contact to it.

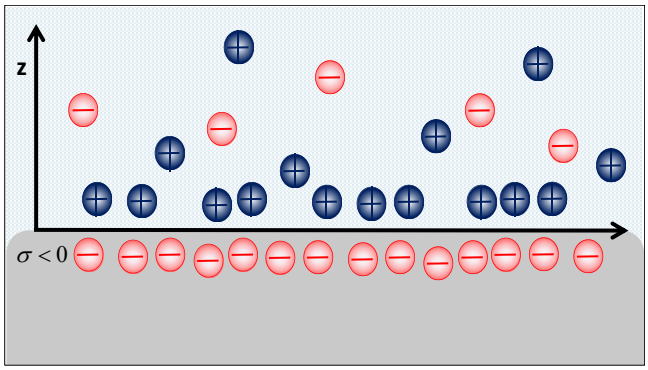

Figure 2.1: Diagram of the electric double layer for a surface with surface charge density σ placed at distance $z = 0$, in contact with an electrolyte bath, so the counterions attracted to the surface create a density profile $n(z)$. The surface is considered an infinite plane.

The first approximation shown in Figure 2.1 contemplates the electric double layer

for a surface with surface charge density σ placed at distance $z = 0$, in contact with an electrolyte bath, so the counterions attracted to the surface create a density profile $n(z)$. Then the potential depends only on the vertical distance from the solid boundary, $\phi(z)$. At the surface it satisfies the electrostatic boundary condition

$$\frac{d\phi}{dz}\Big|_{z=0} = -\frac{1}{\varepsilon}\sigma > 0 \tag{2.8}$$

The equation 2.6 can be integrated, considering a electrolyte with $z_\pm = \pm 1$ and the bulk electrolyte concentration $n_\pm = n_0$, leading to

$$\phi = -\frac{2k_BT}{e}\ln\frac{1+\gamma e^{-z/\lambda}}{1-\gamma e^{-z/\lambda}} \tag{2.9}$$

the new parameter λ is the so called Debye screening length

$$\lambda = \sqrt{\frac{\varepsilon K_B T}{2e^2 n_0}} = \sqrt{\frac{1}{8\pi l_B n_0}} \tag{2.10}$$

Which is the distance where the screening of the electric field occurs. And the definition for the parameter γ is

$$\gamma = -\frac{b}{\lambda} + \sqrt{\left(\frac{b}{\lambda}\right)^2 + 1} \tag{2.11}$$

The coefficient b is known as the *Gouy-Chapman length*, a distance that is inversely proportional to the surface charge density σ,

$$b = \frac{\varepsilon k_B T}{2\pi|\sigma|} = \frac{e}{2\pi l_B|\sigma|} \tag{2.12}$$

And describes that, at a distance b from the surface, the layer of counter-ions will have a total charge of $|\sigma|/2$. In addition from equation 2.5 the ionic densities are:

$$n_\pm = n_0\left(\frac{1 \pm \gamma e^{-z/\lambda}}{1 \mp \gamma e^{-z/\lambda}}\right) \tag{2.13}$$

On Figure 2.2 we present the potential, electric field ($E = -\nabla\phi$) and ion profile (n_+ and n_-) for a surface density of $\sigma = -e/25\text{Å}^2$. This figure shows clearly the accumulation of of counter-ions against the negative charged-wall forming the diffuse layer that reach a limiting value at the wall (n_0).

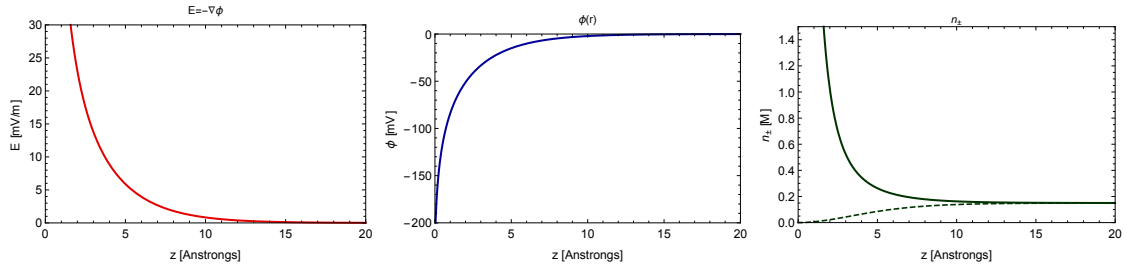

(a) (b) (c)

Figure 2.2: Electric double layer for a surfaces in contact with an electrolyte bath at an electrolyte bulk concentration of n_0=0.1M ($\lambda \approx 2.58$nm) and surface charge at the surface of $\sigma = -e/25\text{Å}^2$.(a) Potential profile ϕ as a function of distance z (b) The electric field profile $E = -\nabla\phi$ that decays to zero for $z \to \infty$ and (c) Ionic density profile of co-ions and counterions where n_+ is the solid line and n_- the dashed line.

Both the Electric field and the electrical decay exponentially and falls off to zero for distances larger than the Debye length ($z \gg \lambda$).

A case that we are more interested in studying is the interaction between **two planar surfaces** (see Figure 2.3), that are equally charged, with a charge density $\sigma < 0$ and that are located at a distance $z = h/2$. These two plates confine a electrolyte therefore they experience forces from the solution.

As it has been mentioned before, when the system is in contact with an electrolyte solution the Poisson-Boltzmann equation takes the form 2.7

$$\nabla^2\phi = \lambda^{-2}\sinh\phi \tag{2.14}$$

In addition, by considering a monovalent electrolyte ($z_\pm = \pm 1$), the electrostatic potential is symmetric at the mid-plane $z = 0$ hence the electric field at this reference point is zero. This allows to study the system only considering the range that goes from $z = 0$ to $z/2$

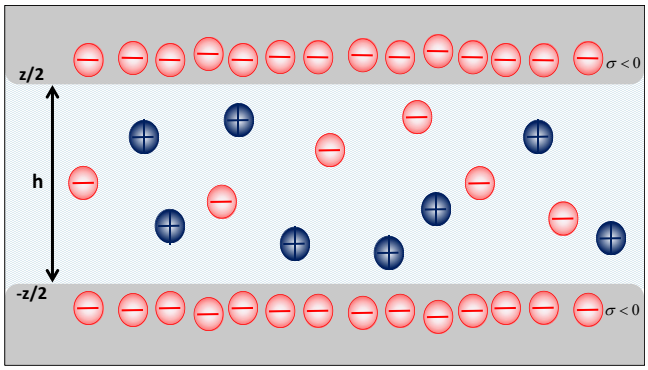

Figure 2.3: Diagram of the electric double layer for a two-surface system. The planar symmetrically charged surfaces are separated by a distance h and located at $z = \pm h/2$. The surface charge is neutralised by the ions in the fluid.

and with the boundary conditions

$$\frac{d\phi}{dz}\Big|_{z=h/2} = \frac{4\pi l_B \sigma}{e} \quad \text{and} \quad \frac{d\phi}{dz}\Big|_{z=-h/2} = -\frac{4\pi l_B \sigma}{e} \tag{2.15}$$

The first integration from $z = 0$ to any point z in between the plates has a solution of the form

$$\lambda \frac{d\phi}{dz} = \sqrt{2\cosh\phi(z) - 2\cosh\phi_{z=0}} \tag{2.16}$$

By rewriting z as a function of ϕ ($z = z(\phi)$), an expression for z is obtained as the second integral of equation (2.16)

$$\frac{z}{\lambda} = \int_{\phi_{z=0}}^{\phi} \frac{d\eta}{\sqrt{2\cosh\eta - 2\cosh\phi_{z=0}}} \tag{2.17}$$

Which does not have a closed form analytical solution, instead the solution can be expressed in terms of elliptic functions, that can be written as

$$F(\theta|\alpha^2) \equiv \int_0^{\theta} \frac{d\eta}{\sqrt{1 - \alpha^2 \sin^2\eta}} \tag{2.18}$$

That by definition $m = e^{\phi_{z=0}}$ and $q = \sin^{-1}(e^{((\phi-\phi_{z=0})/2)})$ leads to

$$z = 2\lambda\sqrt{m}\left[F\left(\frac{\pi}{2}\middle|m^2\right) - F(q|m^2)\right] \tag{2.19}$$

By inverting equation (2.19), the solution for the electrostatic potential

$$\phi = \ln(m) + 2\ln\left[\mathrm{cd}\left(\frac{z}{2\lambda\sqrt{m}}\middle|m^2\right)\right] \tag{2.20}$$

Where cd is known as a Jacobi elliptic function [58–60].

Jacobi functions are a set of basic elliptic functions that in contrast with trigonometric functions, are defined with reference to a circle, the Jacobi elliptic functions are a generalization which refer to other conic sections, the ellipse in particular[62, 63].

One of the basic differences between trigonometric and elliptic functions is that the first depends one one argument only, while Jacobi have two variables. The angle u and the elliptic modulus k that corresponds to the eccentricity of the ellipse, both arguments can be complex or real.

With this two arguments, Jacobi elliptic functions are given by

$$\begin{aligned}
\mathrm{sn}(u|k) &= \sin\alpha \\
\mathrm{cn}(u|k) &= \cos\alpha = \sqrt{1-\mathrm{sn}^2(u|k)} \\
\mathrm{dn}(u|k) &= \sqrt{1-k\mathrm{sn}^2(u|k)} \\
&\text{and} \\
\mathrm{cd}(u|k) &= \frac{\mathrm{cn}(u|k)}{\mathrm{dn}(u|k)}
\end{aligned} \tag{2.21}$$

Where α is known as the Jacobi amplitude and is given by the incomplete elliptical integral given in equation (2.18).

As an example on Figure 2.4 we present a typical counter-ion profile with its corresponding electrostatic potential and electric field for $\sigma = -e/25\text{Å}^2$ and d=0.3 nm.

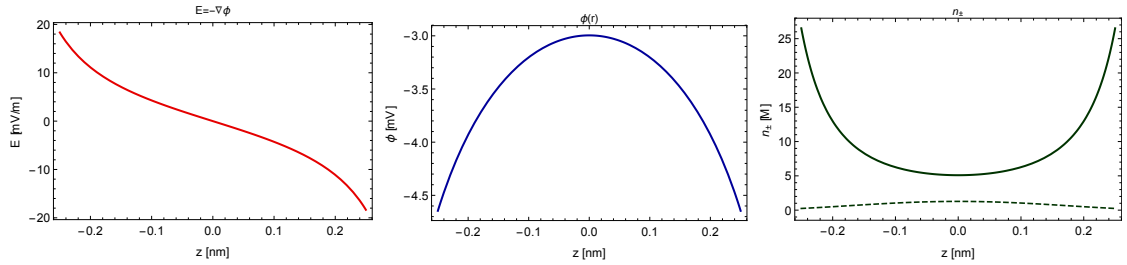

(a) (b) (c)

Figure 2.4: Electric double layer for a surfaces in contact with an electrolyte bath at an electrolyte bulk concentration of n_0=0.7mM ($\lambda = 30nm$) and surface charge at the surface of $\sigma = -e/25$Å.(a) Potential profile ϕ as a function of distance z (b) The electric field profile $E = -\nabla\phi$ that decays to zero for $z \to 0$ and (c) Ionic density profile of co-ions and counterions where n_+ is the solid line and n_- the dashed line.

2.2 Onsager relations

When two or more irreversible transport processes like the exchange of mass, energy, charge or momentum take place at the same time in a thermodynamic system, the processes may interfere with each other. In his work, Onsager [64, 65] assumes that as an analogy to the reciprocal relations that connect forces and displacement complementary relations could exist for transport phenomena. He express the equality of certain ratios between flows and forces in thermodynamic systems out of equilibrium, but where a notion of local equilibrium exists under the assumption of microscopic reversibility. According to this principles at equilibrium, any molecular process and its reverse happen with equal rates [66].

By considering a set of thermodynamic fluxes J_i as a linear functions of thermodynamical forces X_i as

$$J_i = \sum_{j=1}^{n} L_{ij} X_j \tag{2.22}$$

Where L_{ij} measures how rapidly a perturbed system returns to equilibrium (transport coefficients). Then if each flux J_i is the change in time of a thermodynamic variable a_i which in turn is an even function of the velocities of the atoms that conform the system

[67].

In his work Onsager demonstrates that the crossed coefficients L_{ij} and L_{ji} are equal. The fact that they are proportional comes from the fact that both coefficients are measured in the same units.

We want to apply the same principle in the system of interest, where we rely on Poisson-Boltzmann mean-field theory discussed at the beginning of this section and on coupled linear relations for charge and hydrodynamic flows, including electro-osmosis and charge advection described mathematically by the previously mentioned crossed coefficients.

Advection of the mobile charges in the diffuse layer couples the Poiseuille flow to electro-kinetic phenomena. In particular, the advected counter-ions give rise to a radial electric field E, which in turn drives an electro-osmotic flow and electrophoresis of the mobile ions [68] both E and P depend on the radial coordinate r only. In lubrication approximation, the radial velocity satisfies 1D Stokes equation

$$\eta \partial_z^2 v = \nabla P - ecE, \tag{2.23}$$

where P is the hydrodynamic pressure and E the radial electric field induced by the charge displacement. We use the shorthand notation $c = c_+ - c_-$ for concentration difference of positive and negative ions.

The solution for (2.23) can be written as the sum of a pressure driven term and an electro-osmotic term by the velocity field,

$$v(z) = v_P(z) + v_E(z). \tag{2.24}$$

and the charge current

$$j(z) = j_P(z) + j_E(z). \tag{2.25}$$

Even when the surface does not bear free electric charges, polarization charges at the interface between of the surface and the electrolyte caused by the electric field generate

an electrostatic interaction which causes an additional effect to the osmotic pressure on the sphere. In addition, the charges on the surface attract counter-ions, these charges will cause an increment on the ion concentration near the sample that will cause an osmotic pressure repelling the sphere.

This coupled problem is best put in terms of the radial volume and charge flows by integrating both the velocity field (2.24) and the charge current (2.25) along the distance between the sphere and plane that constrict the fluid, i.e. over the vertical variable z,

$$J_V = \int dz(v_P + v_E) = -L_{vv}\nabla P + L_{vc}eE, \tag{2.26}$$

$$J_C = \int dz(j_P + j_E) = -L_{cv}\nabla P + L_{cc}eE, \tag{2.27}$$

The coupled equations (2.26) and (2.27) describe the local non-equilibrium properties in terms of the charge current j and the radial electric field E. Where the generalized forces are $-\nabla P =$ and eE while the transport coefficients L_{ij} represent the pressure-driven volume flow L_{vv} the electrical conductivity L_{cc}, and where the Onsager reciprocal coefficients L_{vc} and L_{cv} describe electro-osmotic flow and pressure-induced charge current, respectively. And due to the Onsager's theory L_{vc} and L_{cv} must be identical.

The first term in equation (2.26) arises from the pressure driven flow profile $v_P(z)$. Assuming no-slip boundary conditions $v_P(\pm h/2) = 0$, and in absence of charge effects ($E = 0$) the Stokes equation $\eta\partial_z^2 v = \partial_r P - \rho E$, the radial Poiseuille flow resulting from the pressure gradient reads as

$$v_P = -\frac{h^2 - 4z^2}{8\eta}\nabla P, \tag{2.28}$$

Where η the fluid viscosity. The Poiseuille flow velocity profile is shown in figure 2.5, with no-slip condition the velocity is zero at the walls and reaches a maximum at the center of the channel. And if we integrate over the vertical variable, it results in

$$\begin{aligned} L_{vv} &= \int dz v_P(z)/\nabla P \\ &= \frac{1}{2}\int_{-h/2}^{h/2} dz z(h-z) = \frac{h^3}{12}. \end{aligned} \tag{2.29}$$

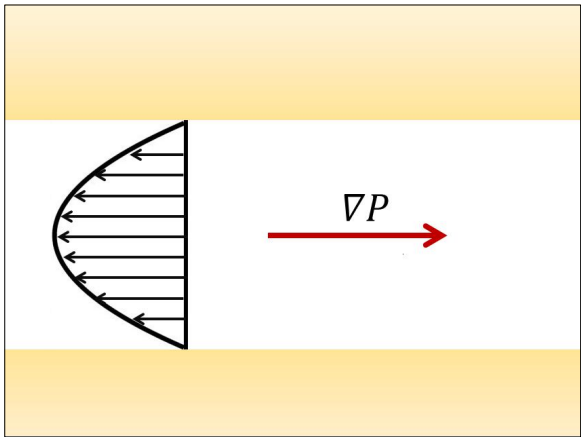

Figure 2.5: Axial velocity profile or a radial Poiseuille flow resulting from the pressure gradient and describes the contribution of the coefficient L_{vv}

The electric field generated moves parallel to the surface and induces a movement of the diffuse layer which drags the rest of the fluid by viscosity, thus creating the so-called the electro-osmotic flow.

As discussed in the section (1.2) far from the surface, the liquid reaches a limiting velocity called the electro-osmotic velocity v_{eo}, that can be derived from the Stokes equation, that when absence of the gradient of pressure is considered, the Stokes equation writes as

$$\eta \frac{\partial^2 v}{\partial z^2} + \rho E = 0 \tag{2.30}$$

In this case ρ is the volumetric charge density and E the electric field. Using the Poisson equation (2.3) by double integrating (2.30) and applying no-slip boundary conditions $v_P(\pm h/2) = 0$ the velocity profile that is obtained from Anderson et al. [69] reads like

$$v_E = \frac{\epsilon}{\eta} \int_z^{h/2} dz' \int_0^{z'} dz'' \rho(z'') E = \frac{\epsilon}{\eta} \left(\psi(z) - \zeta\right) E, \tag{2.31}$$

where the second identity follows from twice integrating Gauss' law $\epsilon \partial_z^2 \psi = -\rho$. This velocity profile mirrors the electrostatic potential profile and is therefore related to the ion density profile.

The velocity v_E relies on the assumption of equally charged upper and lower surface. Then the velocity profile is symmetric with respect to mid plane, and v_E vanishes at both $z = 0$ and $z = h$ with the surface potential $\zeta = \psi(h/2)$, and leads to the transport coefficient L_{vc} shown in the Figure 2.6, here one can observe that at the center of the capillarity, the velocity of the flow dragged due to electro-osmosis is constant

$$\begin{aligned} L_{vc} &= \int dz v_E(z)/E \\ &= \frac{\epsilon}{\eta} \int dz \left(\psi(z) - \zeta\right). \end{aligned} \tag{2.32}$$

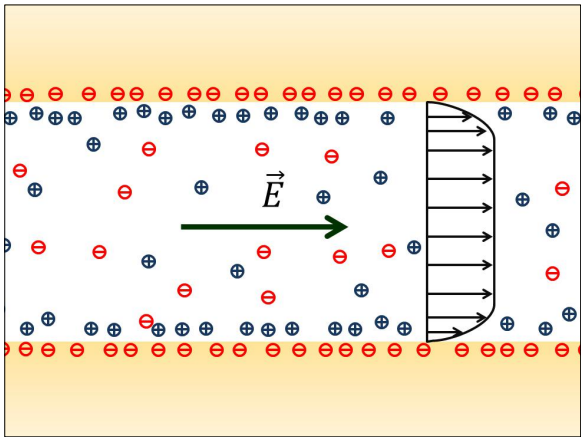

Figure 2.6: Electro-osmotic transport. The net electric density in the diffuse layer is non-zero and a total force is applied to this layer. Due to the viscosity, the ions drag the whole fluid. The contribution is given by the coefficient L_{vc}

Just as due to electro-osmotic transport an electrical potential difference induces flow, a pressure gradient ∇P can induce an electrical current when double layers are involved.

As shown in Figure 2.7, the Poiseuille flow advects the ions present in the diffuse double layer, and since there is an excess of counter ions with respect to the co-ions, a global flow of charges occurs

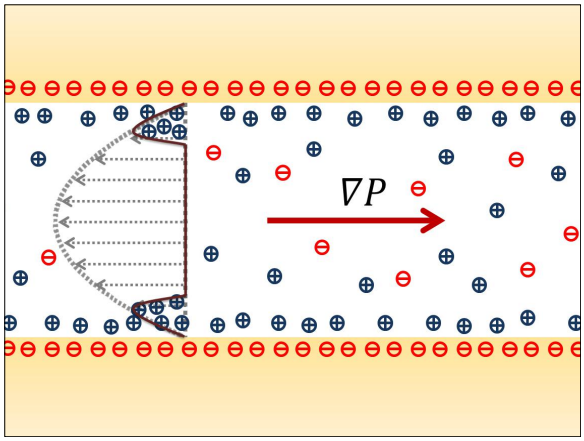

Figure 2.7: Advected charges due to osmotic pressure or flow current. When the fluid is set in motion in a channel whose walls are charged, the counter ions are also displaced, inducing a movement of non-zero charge. Described by the transport coefficient L_{cv}

The described electric current (2.27) consists of advection of counterions in the Poiseuille flow profile v_P,

$$\begin{aligned} L_{cv} &= \frac{1}{\eta}\int dz\rho(z)v_P(z) \\ &= \frac{1}{\eta}\int dz\rho(z)\frac{h^2-4z^2}{8}, \end{aligned} \tag{2.33}$$

To close the system the current density comes from the Ohm's law, the counterions in the diffuse layer are drag due to the accumulation of counter-ions that induces an electric field creating an electric current in the same direction that the electric field (see Figure 2.8) This conductivity is defined by the coefficient

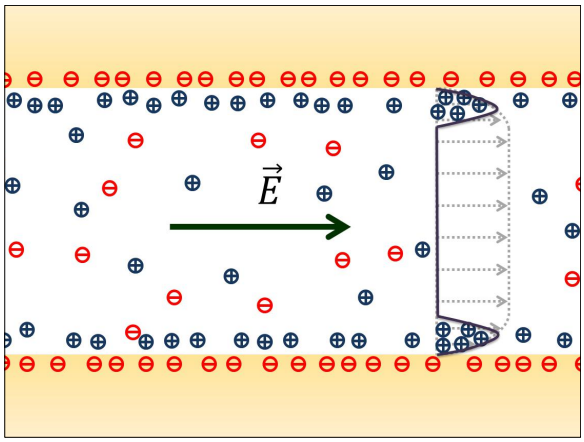

Figure 2.8: Electrical conductivity where a electric field will induce a charge gradient in the double layers and thus a drag-out effect creating flow in the double layer, it gives the contribution of the coefficient L_{cc}

$$\begin{aligned} L_{cc} &= \int_{-h/2}^{h/2} dz \rho(z) v_E(z) + he\mu(n_+ - n_-) \\ &= \int dz \left(\rho \frac{\epsilon}{\eta} (\psi - \zeta) + \mu e^2 (n_+ + n_-) \right) \end{aligned} \tag{2.34}$$

that comprises both advection by the electro-osmotic velocity field v_E and electrophoresis of salt ions [70]. The excess conductivity with respect to the bulk conductivity $2\mu n_0 h$ are often expressed in terms of the Dukhin number [12, 71]. We assume the identical mobilities, $\mu_\pm \equiv \mu$; the general case would require to add a "chemical" contribution to the electric field, proportional to $(\mu_+ - \mu_-)\nabla \ln n$, with the salinity n [69].

Advection-diffusion equation

The radial charge current density is given by

$$j = -D\nabla c + cv + n\mu E, \tag{2.35}$$

where c is the charge concentration, n the salinity, $D = \mu k_B T$ the ion diffusion coefficient, and v the radial velocity profile, as mentioned before, we assume identical mobilities, μ.

This equation is closed by the continuity equation for the ion current

$$\nabla \cdot j = -e\partial_t c, \tag{2.36}$$

In addition, a relation between the distribution of electric charge and the resulting electric field is required, considering the full volume enclosed between the charged surfaces. The Gauss' law relating the radial electric field E and the non-equilibrium charge density,

$$\nabla \cdot E = e(c - c_0)/\varepsilon, \tag{2.37}$$

where $c - c_0$ is the deviation from the equilibrium charge density ec_0. Here the equilibrium value is related to the Poisson-Boltzmann potential ψ resulting from the surface charges [58–60, 72],

$$\partial_z^2 \psi = ec_0/\varepsilon. \tag{2.38}$$

We are interested in a water film between surfaces of low-permittivity materials such as silica or mica. In this case, the electric field has a radial component only, it hardly penetrates the boundaries and thus is constant with respect to z. With the vertical integral of the charge density,

$$C = \int_0^h dz c,$$

the continuity equation (2.36) becomes

$$\partial_t C = D\nabla^2 C - \nabla \cdot J_C, \tag{2.39}$$

In this chapter we describe the electroviscous phenomena resulting from charge-flow coupling in a nanoscale capillary, starting from the Poisson-Boltzmann mean-field theory and the coupled linear relations for charge and hydrodynamic flows, including electro-osmosis and charge advection.

Chapter 3

Electroviscous drag force in the steady state

This chapter aims to investigate some of the basic behavior of an aqueous solution trapped between two charged surfaces, formed by a sphere of radius R and a substrate in a quasistatic state, where the relaxation rate is much larger than the typical oscillation frequencies of the sphere. This chapter aims to investigate some of the basic behavior of an aqueous solution trapped between two charged surfaces, formed by a sphere of radius R and a substrate in a quasistatic state, where the relaxation rate is much larger than the typical oscillation frequencies of the sphere.

3.1 Setting the problem

Consider a charged surface in contact with an electrolyte solution as displayed in figure 3.1. The surface has a diffuse layer confined by a vibrating sphere, also charged, of radius R mounted on the cantilever of an AFM [21, 73]. The sphere is treated as a flat interface since the radius is much larger than the distance at which the fluid is confined. These surfaces as also considered to be uniformly charged (constant surface charge distribution). The mobile charges are distributed continuously along with the fluid and we considered only the properties in thermodynamic equilibrium [60].

As displayed in the diagram 3.1, the vertical position of the sphere oscillates with a velocity $V(t)$ according to $A\sin(\omega t)$, resulting in the velocity proportional to the amplitude and frequency of the oscillation,

$$V(t) = A\omega\cos(\omega t), \tag{3.1}$$

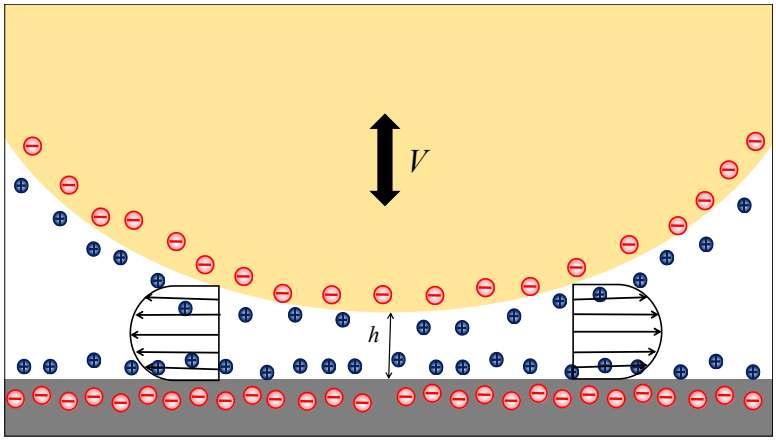

Figure 3.1: Diagram of the experimental system. A sphere of radius R oscillates with a velocity $V = A\omega\cos(\omega t)$ at a distance h, from a charged surface. The polarized charges on the surface of both the substrate and the sphere interact with the charges in the fluid.

The oscillation of the sphere induces a non-uniform hydrodynamic pressure P in the film and imposes a flow J_V as shown schematically in Fig. 3.1. For an incompressible fluid, there is a simple geometrical relation between the vertical velocity of the tip of the cantilever and the volume flow J_V carried by the radial fluid velocity $v(z,r)$,

$$\pi r^2 V = 2\pi r J_V = 2\pi r \int_h dz v(z,r). \tag{3.2}$$

The film thickness being much smaller than the curvature radius, we resort to the lubrication approximation [74], thus simplifying significantly the fluid mechanical problem. For distances h much smaller than the radius of the oscillating sphere, the vertical distance between the two boundaries $h = h_0 + R - \sqrt{R^2 - r^2}$ is well approximated by

$$h = h_0 + \frac{r^2}{2R}, \qquad (r \ll R).. \tag{3.3}$$

when this is valid, the hydrodynamic pressure P is independent of z hence the vertical component of the velocity field is negligible, and the radial component $v = v(z, r)$ obeys a simplified Stokes equation,

$$\eta \partial_z^2 v = \partial_r P - \rho E, \tag{3.4}$$

with the viscosity η and where only the vertical component of the Laplace operator $\nabla^2 v$ has been held. The right-hand side comprises the radial pressure gradient $\partial_r P$ and the force exerted by a radial electric field E and the charge density ρ of the diffuse layer.

3.2 Stationary case

Electrokinetic phenomena in a channel between two electrolyte reservoirs at different electrochemical potential, are characterized by a constant streaming current $J_C \neq 0$ [2, 34, 75]. On the contrary if one considers a open geometry, where the fluid in the capillarity is in contact with air and, as is our case of study, it is within a periodically driven squeezing motion, it will not not allow for a steady current but given the accumulation of counterions, it gives rise to the electric field E.

Strictly speaking, there is a small current which develops the space charges related to the electric field,

$$\delta\rho = \epsilon \nabla \cdot E. \tag{3.5}$$

and which vanishes when averaged over one cycle. Because of the strong electric interactions, the space charges develop almost instantaneously such that the electric field is in phase with the pressure gradient, and that advection and conduction currents cancel each other in the charge flow as follows:

$$J_C = -L_{cv}\nabla P + L_{cc}eE = 0. \tag{3.6}$$

This relation holds true as long as the charge relaxation time τ is much shorter than the period of the external driven, $\omega\tau \ll 1$. This relaxation time can be obtained from the diffusion equation. As mentioned in the previous chapter the continuity equation takes the form

$$\partial_t C = D\nabla^2 C - \nabla \cdot J_C, \tag{3.7}$$

where the diffusion time of the advected counter-ions occurs on a time scale $\tau_D = Rh_0/D$, of the order of a second, which turns out to be much larger than the time scale arising from the coupled currents allowing to discard the diffusion term, that leads to an expression of the continuity equation as:

$$i\omega E = -\frac{e}{h\varepsilon}J_C. \tag{3.8}$$

That leads to the definition of the charge relaxation rate given by

$$\frac{1}{\tau_c} = \frac{h_0\varepsilon\eta}{e^2 L_{cc}} \tag{3.9}$$

and that it turns out to be much larger than typical oscillation frequencies, since it is in the order of $1/\tau_c \sim 10^5$ s^{-1}, whereas the cantilever frequency, $\omega \sim 10^2$ s^{-1}. This means that the non-equilibrium charge distribution and the corresponding radial electric field E follow the mechanical driving instantaneously, and that the charge current is negligibly small. As a consequence we use the approximation $J_C = 0$ in (2.27) that we review in the previous chapter

$$J_C = -L_{cv}\nabla P + L_{cc}eE, \tag{3.10}$$

we can fin an expression for electric field proportional to the pressure gradient.

$$eE = \frac{L_{cv}}{L_{cc}} \nabla P \tag{3.11}$$

As the radial flow of liquid J_V is fixed

$$J_V = \frac{\eta r V}{2} = -L_{vv} \nabla P + L_{vc} eE, \tag{3.12}$$

we obtain the correction of the Poiseuille flow from the diffuse layer.

$$\nabla P = -\frac{6\eta r V}{h^3} \frac{1}{1-\xi} \tag{3.13}$$

where the coupling of the double layer to the flow is accounted for by the ratio of off-diagonal and diagonal transport coefficients L_{ij}

$$\xi = \frac{L_{vc} L_{cv}}{L_{vv} L_{cc}} \tag{3.14}$$

From (3.13) it is clear that the dimensionless parameter ξ describes the effect of charge-flow coupling on the hydrodynamic pressure. For $\xi = 0$ one recovers the well-known expression for the pressure gradient in capillary. The stability of the dynamic equations (2.26) and (2.27) requires a positive determinant of the transport matrix, $\det \mathbf{L} > 0$ or $\xi < 1$.

In lubrication approximation where the height $h(r)$ varies with the radial position according to $h = h_0 + r^2/2R$. Therefore when integrating the excess hydrodynamic pressure in the capillary, it turns out convenient to use the variable h instead of r so one has $dh = drr/R$ and the hydrodynamic pressure takes the form

$$P(h) = 6\eta V \int_h^\infty \frac{dh'}{h'^3} \frac{1}{1-\xi(h')}. \tag{3.15}$$

Finally, the viscous force on the cantilever is given by the surface integral of the pressure. With $dS = 2\pi drr$ and by regritting everything in terms of the height h we get $dS = 2\pi R dh$ and one finds

$$F = \int dS P(r) = 2\pi R \int_{h_0}^\infty dh P(h). \tag{3.16}$$

As a first approach we considered the simplest case, we solve in the absence of electroviscous coupling this means that the correction term $\xi = 0$, one readily obtains the pressure

$$P_0(h) = \frac{3}{2}\eta V R/h^2 \tag{3.17}$$

which is maximum at the centre of the film and vanishes as $P \propto r^{-4}$ at large radial distance. Performing the surface integral one obtains the lubrication drag force [43]

$$F_0 = \frac{6\pi\eta V R^2}{h_0}, \quad (\xi = 0), \tag{3.18}$$

that is by a factor R/h_0 larger than the Stokes drag on a sphere of radius R in a bulk liquid. Equation (3.16) expresses the electroviscous drag enhancement in terms of the coupling coefficient ξ which quantifies the charge-flow coupling. In the sequel, we evaluate this enhancement as a function of the height of the channel compared with the Debye length, considering a narrow channel when the height $h \ll \lambda$ and a wide channel if $h \gg \lambda$.

3.3 Wide channel approximation

If a width of the water film is much larger than the Debye length, $h \gg \lambda$, then the mid plane potential vanishes, giving a solution for the electrostatic potential [59]

$$\psi = -\frac{4k_B T}{e}\text{arctanh}(\gamma e^{-z/\lambda}), \tag{3.19}$$

with $\gamma = \sqrt{1+q^2} - q$ and $q = 1/2\pi\sigma\ell_B\lambda$. In this case, there are analytical expressions for the transport coefficients L_{ij}. The off-diagonal term L_{vc} caused by electro-osmosis is given by the Helmholtz-Smoluchowski electrophoretic mobility. Recalling equation (2.33)

$$L_{vc} = \frac{\epsilon}{\eta}\int dz\,(\psi(z) - \zeta)\,. \tag{3.20}$$

and inserting the definition of the electrostatic potential, one gets

$$L_{vc} = -\frac{h\varepsilon\zeta}{e\eta} = -\frac{h\hat{\zeta}}{4\pi l_B} \tag{3.21}$$

Where we have introduced the reduced zeta potential $\hat{\zeta} = 2\zeta/k_BT$ in units of the thermal energy. The solution for the electrical conductivity is

$$L_{cc} = \frac{\sinh\left(\frac{1}{4}\hat{\zeta}\right)^2}{\lambda\pi^2 l_B^2\eta} + 2\mu(\sigma + n_0 h) \tag{3.22}$$

The last term $2\mu n_0 h$ is the bulk conductivity of the electrolyte solution, whereas the first two terms account for surface corrections, which comprise counter-ion electrophoresis $\propto \sigma$ and electro-osmotic advection.

The volume flow driven by electro-osmosis is well approximated by the product of slip velocity and channel width. Thus, neglecting boundary effects, the electric current L_{cv} turns out to be identical to L_{vc},

$$L_{cv} = -\frac{h\varepsilon\zeta}{e\eta} \tag{3.23}$$

For wide channels, the conductivity is dominated by ion electrophoresis, $2\mu(\sigma+n_0h_0)$, such the electro-osmotic term may be discarded. With the definition of the screening length

$$\frac{e}{k_BT}\frac{d^2\psi}{dz^2} = \lambda^{-2}\sinh\frac{e\psi}{k_BT}, \tag{3.24}$$

the coupling parameter simplifies, if we rewrite the ion mobility as $\mu = 1/6\pi\eta a$ with the hydrodynamic radius a we obtain the electroviscous coupling parameter

$$\xi = \frac{3\lambda}{4h}\frac{\hat{\zeta}^2}{\sinh\left(\hat{\zeta}/4\right)^2 + \frac{\sigma+n_0h}{3a}\pi\lambda l_B^2} \tag{3.25}$$

The behavior of ξ still depends on the ratio of the bulk conductivity proportional to n_0h and surface contributions which comprise counter-ion electrophoresis $\propto \sigma$ and electro-osmotic advection. It turns out that the latter term may be neglected for the most relevant situations. After rearranging the remainder and using the definition of the screening length,

the electroviscous coupling parameter reads as

$$\xi(x) = \frac{\lambda_*^2}{2h^2}\frac{1}{1+x}, \tag{3.26}$$

where we have defined the length scale

$$\lambda_* = 6\hat{\zeta}\sqrt{\frac{a}{\ell_B}}\lambda \tag{3.27}$$

and the ratio of surface and bulk conductivities,

$$x = \frac{\sigma}{hn_0}. \tag{3.28}$$

In the following we first discuss the case where surface conductivity is not relevant $x \ll 1$ and then account the effect of surface conductivity.

Surface conductivity effect

Force for limiting case $n_0 h/\sigma \gg 1$

As a first approach to the problem, we discard the surface conductivity and set the coefficient $x = 0$. Then the pressure and the viscous force can be integrated in closed form,

$$P = \frac{3\eta V R}{\lambda_*^2}\ln\left(1 - \frac{4\lambda_*^2}{h}\right). \tag{3.29}$$

And the total force

$$\frac{F}{F_0} = \frac{h_0}{\lambda_*}\ln\frac{h_0+\lambda_*}{h_0-\lambda_*} + \frac{h_0^2}{\lambda_*^2}\ln\frac{h_0^2-\lambda_*^2}{h_0^2} \tag{3.30}$$

As it has been previously discussed, the prefactor F_0 refers to the visco-elastic force in the absence of charge effects:

$$F_0 = -\frac{6\eta V R^2}{h_0} \tag{3.31}$$

It turns out instructive to rewrite (3.30) as a series in powers of λ_*/h_0,

$$\frac{F}{F_0} = 1 + \frac{1}{6}\frac{\lambda_*^2}{h_0^2} + \frac{1}{15}\frac{\lambda_*^4}{h_0^4} + \frac{1}{28}\frac{\lambda_*^6}{h_0^6} + ... \tag{3.32}$$

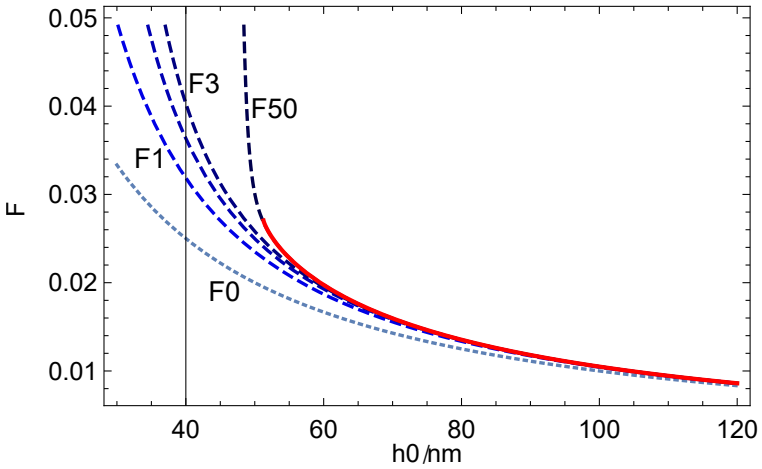

Figure 3.2: Electroviscous enhancement of the drag force , as a function of the reduced sphere-plane distance h_0, in the absence of surface conductivity. The dotted line "F0" gives the force F_0 without electroviscous coupling as in (3.31), dashed lines the perturbation series (3.32) truncated at $(\lambda_*/h_0)^{2n}$ with $n = 1, 2, 3, 50$, and the full line the complete series (3.30), which is not defined for $h < \lambda_*$.

The force F is plotted in Fig. 3.2 as a (red) solid line, which stops at the distance $h_0 = \lambda_*$. At this point the electroviscous coupling parameter ξ is equal to unity and, as a consequence, a logarithmic branch point appears in the pressure integral (3.15), resulting in the value of the force ratio $F/F_0 = 2\ln 2 \approx 1.39$. At smaller distances the pressure and force integrals provide complex numbers which have no physical meaning and consequently the pressure and force are not defined in a wide channel approximation.

We compare this expression with the uncoupled lubrication drag force (3.31). Retaining a few correction terms of the series, suggests a smooth behavior, whereas eq. (3.30) is defined for $h_0 \geq \lambda_*$ only. The first correction term, proportional to λ_*^2/h_0^2, corresponds to the electroviscous coefficient of Bike and Prieve [3].

Noting that the ion radius is usually smaller than the Bjerrum length $\ell_B = 0.7$ nm,

and that the reduced zeta potential $\hat{\zeta}$ is of the order of unity, one finds that λ_*/λ takes values between 1 and 10.

Force for limiting case $n_0 h/\sigma \ll 1$

When the spacing of the channel h_0 is small, the approximation that allowed us to neglect x in (3.26) cannot be consider any more, since there will be interaction between the ions attached to both of the surfaces. However we face the problem that it can not be integrated analytically. In this case there is not a direct analytical solution so as a first approximation we propose to write the first term expansion the pressure gradient as

$$\nabla P = \frac{6\eta r V}{h^3}(1 + \xi(x)) \tag{3.33}$$

Where $\xi(x)$ follows the same definition from equation (3.26), this leads to an expression for the viscous force like

$$F = -\frac{6\pi\eta V R^2}{h_0}(1 + \xi_*) \tag{3.34}$$

With

$$\xi_* = -\frac{\lambda_*^4}{6x^4 h_0^3}\left(6 - x^2 + 3x - 6\left(1 + \frac{1}{x}\right)\ln(1 + x)\right) \tag{3.35}$$

Further study is required for the case where surface conductivity becomes relevant at smaller channel widths, however we show in Figure 3.3 that it may describe a valid behaviour for $h < \lambda_*$.

3.4 Narrow channel approximation

In the case of a narrow channel, $h \ll \lambda$, the overlapping double layers of the surfaces results in a constant charge density

$$\rho = \epsilon \partial_z^2 \psi = \sigma/h, \tag{3.36}$$

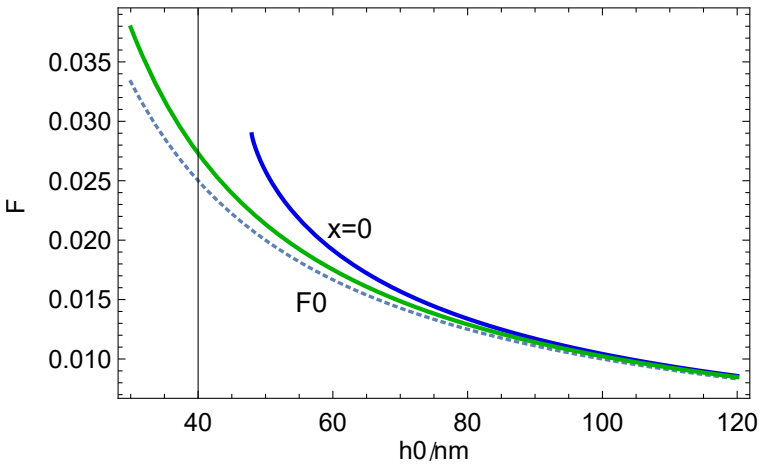

Figure 3.3: Electroviscous enhancement of the drag force, as a function of the sphere-plane distance of closest approach h_0. The dotted line "F0" gives the force F_0 without electroviscous coupling as in (3.31), the force in the absence of surface conductivity "x=0" (blue) (3.30) and with the correction including surface charge (green) (3.34). In contrast with the solution for x=0 (3.34) is defined for $h < \lambda_*$.

in other words, the counterions form a homogeneous gas [59]. The electrostatic potential is readily integrated,

$$\psi(z) = \frac{k_B T}{e}\left(\ln k - \frac{4\pi\ell_B\sigma}{h}z^2\right), \tag{3.37}$$

where the parameter k describes the finite potential at mid-plane $\psi(0) = (k_B T/e)\ln k$.

With these expressions for ρ and ψ the transport coefficients are readily calculated. Retaining contributions up to first order in h only, we find

$$L_{vc} = \frac{\epsilon}{\eta}\int dz\,(\psi(z) - \zeta) = \frac{e\sigma h^2}{12\eta}, \tag{3.38}$$

and that driven by the electric field,

$$L_{cc} = \int dz\left(\rho\frac{\epsilon}{\eta}(\psi - \zeta) + \mu e^2(n_+ + n_-)\right) = \frac{e^2\sigma^2 h}{12\eta} + \frac{e^2(\sigma + n_0 h)}{3\pi a\eta}, \tag{3.39}$$

Therefore the coupling coefficient can be expressed as

$$\xi = \frac{L_{vc}L_{cv}}{L_{vv}L_{cc}} = \frac{\pi\sigma^2 ah}{\pi\sigma^2 ah + 4(\sigma + n_0 h)} \tag{3.40}$$

It is important to note that ξ is independent of the Debye length. For narrow channels, the denominator takes the value 4σ, and ξ decreases linearly with h. This gives an expression for the viscoelastic force

$$F = -F_0\left(1 - \frac{ah_0\pi\sigma}{2} - \frac{ah_0\pi(h_0 n_0 + 2\sigma)}{4}\ln\left(\frac{h_0 n_0}{h_0 n_0 + 2\sigma}\right)\right) \tag{3.41}$$

That as it is displayed in Figure 3.4, will increase as a function of the surface conductivity.

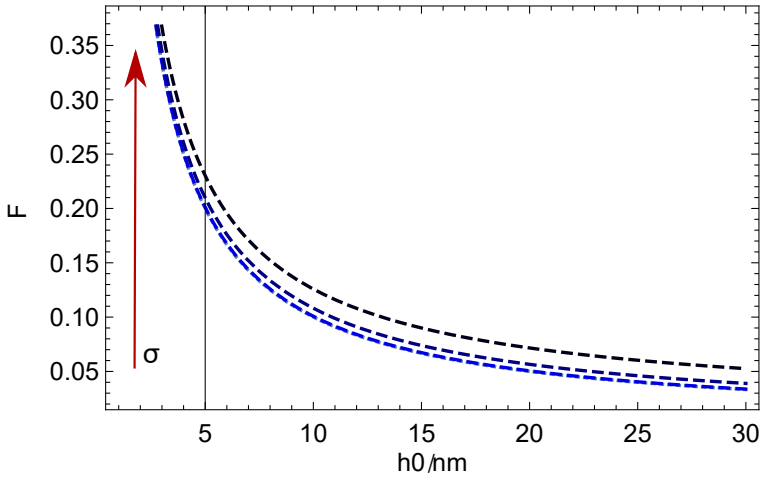

Figure 3.4: Electroviscous enhancement of the drag force, as a function of the sphere-plane distance of closest approach h_0 for a narrow channel. The dotted lines are the force (3.41) calculated for increasing values of surface conductivity.

3.5 Numerical evaluation of ξ

In the general case, the electrostatic potential is obtained in terms of the Jacobi elliptic function $\mathrm{cd}(u|m)$ discussed in the chapter 2 in equation (2.21) [76],

$$\psi(z) = \frac{k_B T}{e}\left[\ln k + 2\ln \mathrm{cd}\left(\frac{z}{2\lambda\sqrt{k}}\middle| k^2\right)\right]. \tag{3.42}$$

This potential is completely determined by the density profiles that are function of the physical parameters, the distance between the surfaces h, the charge density σ and the bulk density n_0. Because of $\mathrm{cd}(0|m) = 1$, the second term vanishes at $z = 0$, and the potential at mid-plane is given by $\ln k$. The parameter k depends on the ratio of the channel width and the Debye length as well as the surface conductivity σ as shown in Figure 3.5

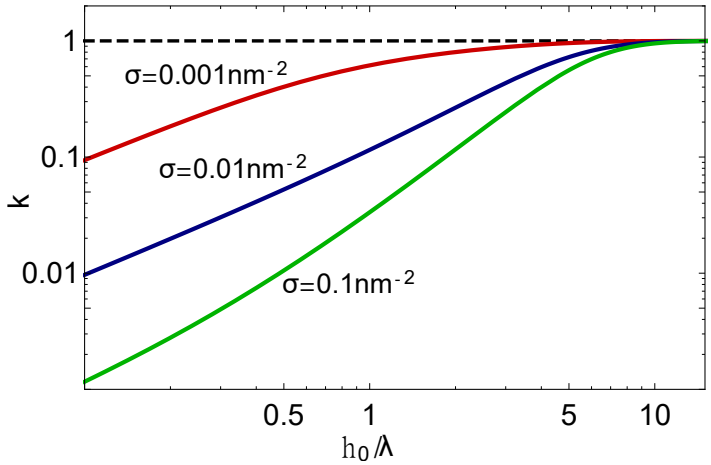

Figure 3.5: The parameter k of the electrostatic potential (3.42) as a function of reduced channel width h/λ, for three values of the surface charge density σ; for distances larger than λ_*, that is, $h \gg \lambda$, one reaches the wide-channel limit $k = 1$.

For $h \gg \lambda$ one has $k = 1$ and recovers the analytic expression

$$\psi = -\frac{4k_BT}{e}\mathrm{arctanh}(\gamma e^{-z/\lambda}), \tag{3.43}$$

for a charged surface limiting an infinite half-space. In the narrow-channel limit one finds

$$k = \frac{hn_0}{2\sigma}, \quad (hn_0 \ll \sigma), \tag{3.44}$$

this implies that by expanding the Jacobi function to second order in z, one can recover the narrow-channel electrostatic potential

$$\psi(z) = \frac{k_B T}{e}\left(\ln m - \frac{4\pi\ell_B\sigma}{h}z^2\right). \tag{3.45}$$

To obtained the general solution the electric potential (3.42) is calculated considering a fixed surface charge density $e\sigma$, therefore it satisfies the boundary condition

$$\frac{e\sigma}{\varepsilon} = \mp \left.\frac{d\psi}{dz}\right|_{z=\pm h/2}. \tag{3.46}$$

Then the electroviscous coupling parameter ξ

$$\xi = \frac{L_{vc}L_{cv}}{L_{vv}L_{cc}}. \tag{3.47}$$

is obtained by performing the integrals for the transport coefficients L_{cv}, L_{vc} and L_{cc} for a given film distance h and Debye length λ.

This general solution permits to eliminate the range restriction for the obtained electroviscous coupling, since it can be calculated along all the range of the sphere-plane distance h. We obtained numerical values for the coupling parameter $\xi(h)$ by integrating the transport coefficients using the software *Mathematica* that has a definition of the Jacobi functions. Our Notebook takes an initial value of λ and σ that we fix from the possible physical scenarios observed in experiments and that are considered constant along all the range of heights h evaluated. The success of the calculation depends on a convergence of the solution for the parameter k that as shown in Figure 3.5 is a parameter that must be recalculated for each value of the distance h.

Figure 3.6 shows the variation of ξ as a function of h for different values of surface charge concentration σ and Debye length λ, and compares with narrow-channel (dotted lines) and wide-channel (dashed lines) approximations. First, when the coupling parameter is calculated for different values of σ at a fixed λ as in Figure 3.6(a) we observe a surprising feature, that ξ is roughly linear in σ. From the slope of the log-log plot one finds the power

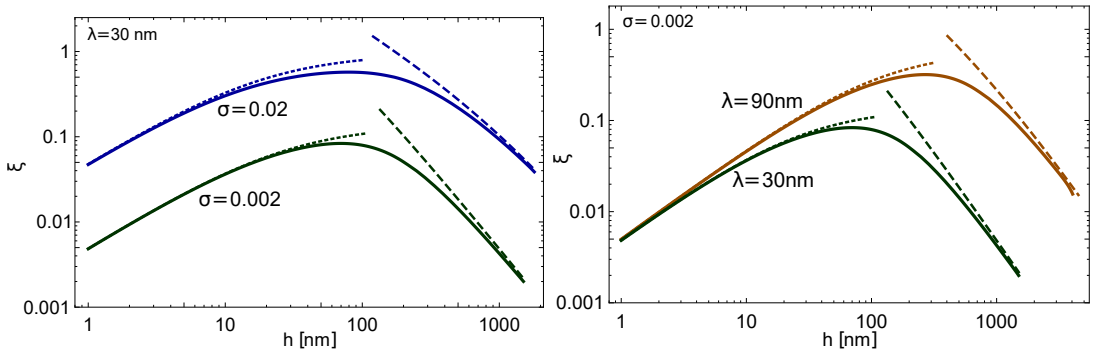

(a) (b)

Figure 3.6: Numerical calculation of the electroviscous coupling parameter ξ as a function of h, for surface charge density $\sigma = 0.002$ and $0.02\,\mathrm{nm}^{-2}$, and Debye length $\lambda = 30$ and 90 nm. Dotted and dashed lines correspond to the approximations of narrow and wide channels, respectively, whereas the solid lines give the numerical solution.

law $\xi \propto h$ and $\xi \propto h^{-2}$ in the limits of narrow and wide channels, respectively.

In addition, from Figure 3.6(b), where λ variate as a function of σ we notice that the maximum of the coupling parameter occurs at $h_{\max} \approx 3\lambda$. The narrow-channel result (3.40) provides a good description for $h \leq \lambda$, whereas the wide-channel expression (3.25) converges for $h \gg \lambda_*$ only. One must conclude that in the intermediate range, which covers at least one decade in h, neither of them is valid.

In Figure 3.7 we plot the enhancement factor $F/F_0 - 1$ of the viscous force

$$F = 2\pi R \int_{h_0}^{\infty} dh P(h). \tag{3.48}$$

With parameters as in Fig. 3.6. As expected for the electroviscous coupling parameter ξ, there is a maximum at $h \approx \lambda$. The enhancement factor depends equally strongly on the surface charge and the Debye length. The upper curve exceeds unity, which means that the force is more than twice F_0.

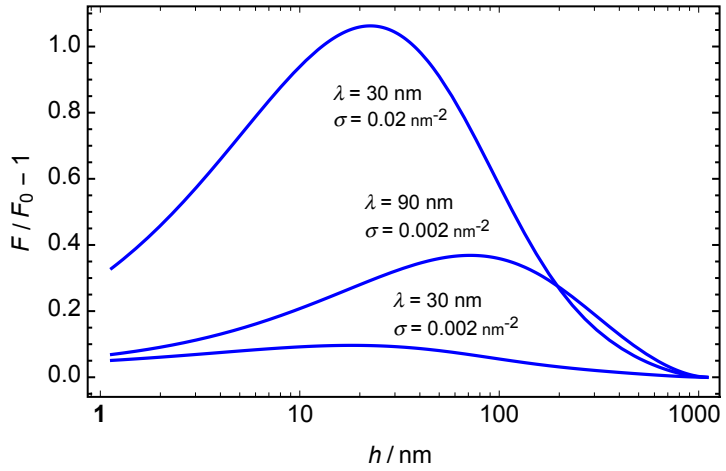

Figure 3.7: Relative electroviscous force $F/F_0 - 1$ as a function of h, for different values of surface charge density σ and Debye length λ.

3.6 Charge regulation

The three most commonly used boundary conditions for charged surface systems are constant charge (cc), constant potential (cp) and charge regulation (cr) [77, 78]. So far we have assumed that the surface charge density σ remains constant upon varying the film thickness h_0, this is the case of constant charge (cc) boundary conditions. In a different approach, one can make the assumption that the ion concentration remains constant near the charged surfaces, implying a constant potential (cp). In this case the boundary condition (3.49)

$$\frac{e\sigma}{\varepsilon} = \mp \left.\frac{d\psi}{dz}\right|_{z=\pm h/2}. \tag{3.49}$$

has a solution for the potential along the channel as

$$\psi(\pm h/2) = \zeta_\infty. \tag{3.50}$$

Here ζ_∞ is the surface potential at large distance, calculated with the surface charge σ according to

$$\psi = -\frac{4k_BT}{e}\text{arctanh}(\gamma e^{-z/\lambda}), \tag{3.51}$$

.

However, neither a constant charge nor a constant potential are the case for ionizable groups at the surface HA which release and recover protons, this effect is known as charge regulation. The surface dissociation and association can be described as

$$\text{HA} \rightleftharpoons \text{H}^+ + \text{A}^-. \tag{3.52}$$

In this reaction H represents a site in the surface that can be negatively charged or neutral, as depicted in Figure 3.8

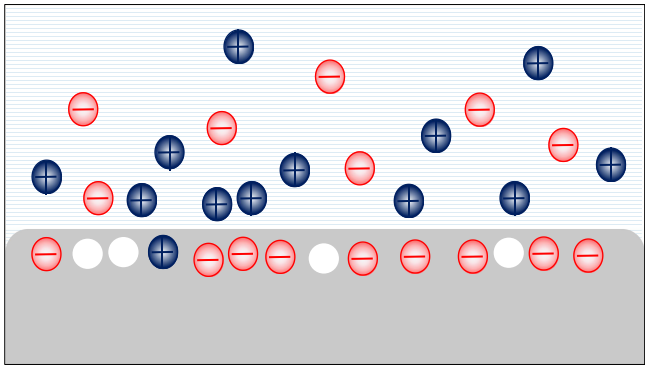

Figure 3.8: Graphic of the effect of charge regulation on a surface with dissociable ionic groups. Some of the acidic groups are released leaving the surface with negative charged sites (red) and uncharged sites (white).

For narrow channels the potential $\psi(z)$ given in (3.42) takes a finite value at mid-plane, $\psi(0) = (k_BT/e)\ln k$, which favors recombination of the surface groups, thus reducing the effective charge density σ and surface potential ζ.

A simple and widely studied model [79, 80] relies on the dissociation constant

$$Z = \frac{[\text{H}^+][\text{A}^-]}{[\text{AH}]} = n_s\frac{\alpha}{1-\alpha}, \tag{3.53}$$

where $[H^+]$, $[A^-]$ and $[AH]$ stand for the three possible surface concentrations. We have defined the dissociated fraction α and the hydronium concentration at the surface

$$n_s = e^{-e\zeta/k_BT}[H^+]_\infty \tag{3.54}$$

Solving for α one finds the fraction of dissociated sites

$$\alpha = \frac{1}{1 + n_s/Z}, \tag{3.55}$$

and the number density of surface charges,

$$\sigma = \frac{\alpha}{S}. \tag{3.56}$$

The electrostatic potential is obtained by closing the above relations with the boundary condition (3.46). The area per site S is chosen such that at large distance (where $\zeta = \zeta_\infty$), σ takes the value indicated for the case of constant charge.

As discussed previously, the parameter k of the electrostatic potential expressed in terms of the Jacobi elliptic functions in equation (3.42) is a function of the reduced channel width h and of the surface charge density σ. In Figure 3.9 we plot k for three values of σ as a function of h/λ considering tree different boundary conditions: constant charge (cc), constant potential (cp), and charge regulation (cr).

We observe that for distances larger than $\lambda_* = 6\hat{\zeta}\sqrt{\frac{a}{\ell_B}}\lambda$, that is, $h \gg \lambda$, one reaches the wide-channel limit $k = 1$, where the electroviscous force component is small. On the other hand, the electrostatic boundary condition and charge regulation are relevant at shorter distances, $h < \lambda$ for weakly charged surfaces and $h \ll \lambda$ for higher surface charge σ.

In order to observe where the effect of charge regulation is valid we compare the electroviscous properties calculated at constant charge with the charge-regulated case, and also with that of constant potential.

In Figure 3.10 we plot the coupling parameter ξ for the cases of constant charge and constant surface potential, and observe a behavior similar to what has been reported

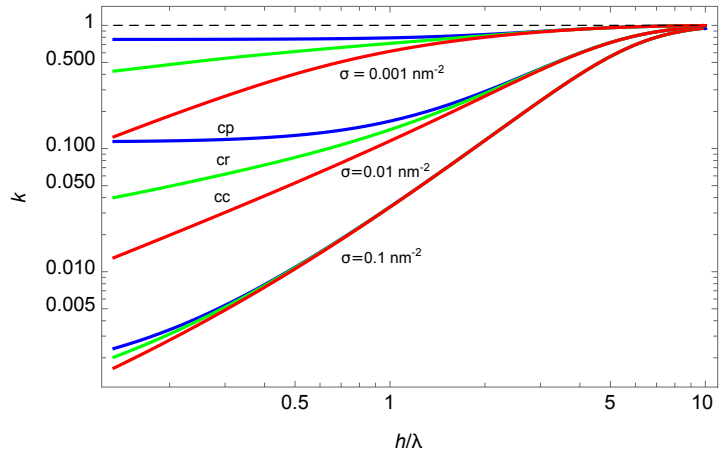

Figure 3.9: Parameter k of the electrostatic potential as a function of reduced channel width h/λ, for three values of the surface charge density σ, where the red line corresponds to the boundary condition of constant charge (cc), the blue line to a constant potential (cp), and the green line represents the charge regulation case (cr).

previously for the disjoining pressure [60]: At distances smaller than the screening length, $h < \lambda$, the curves of ξ for different boundary conditions diverge significantly. Yet note that the electroviscous coupling is strongest in the range $\lambda < h < 10\lambda$, where charge regulation is of little importance.

The electroviscous enhancement of the drag force F with respect to the uncoupled expression F_0 is shown in Figure 3.11. The maximum occurs at a distance slightly below the screening length. For the given electrostatic parameters, it reaches the value $F/F_0 \approx 2$, which depends little on the electrostatic boundary condition.

As discussed for the electroviscous drag component for constant charge density as shown in Figure 3.7, the enhancement of the force disappears at much higher distances of about 10λ.

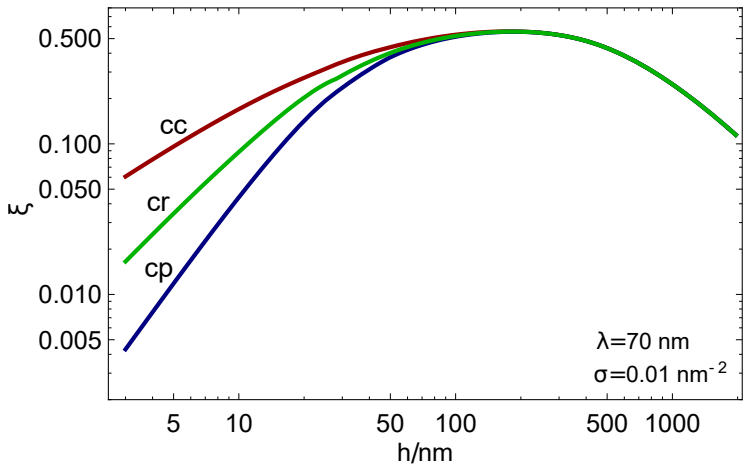

Figure 3.10: Numerical calculation of the electroviscous coupling parameter ξ as a function of h, for an initial surface charge density $\sigma = 0.01$ nm^{-2}, and Debye length $\lambda = 70$ nm for constant charge (cc), charge regulation (cr), and constant potential (cp).

3.7 Static Force

Now we consider the static repulsive force arising from the overlap of the diffuse layers on the opposite surfaces, and which is independent of the external driving.

The disjoining pressure is the distance dependence of the interaction between two surfaces, either attractive or repulsive. It is a pressure due to the attractive force between two surfaces, divided by the area of the surfaces [81].

In the case of a film on a substrate, deGennes defined the energy function P(e) as the excess energy of a film on a substrate as a function of film thickness (e). Derjaguin defined the disjoining pressure as the derivative of this energy P(e) as a function of e. The disjoining pressure is related to the stability of films. When P(e) is a decreasing function of e (favoring a thick film), $\pi(e)$ is positive and the film is considered to be stable.

Then the disjoining pressure is given by the excess osmotic pressure of the mobile ions at midplane,

$$\Pi = (n_m - 2n_0)k_BT \tag{3.57}$$

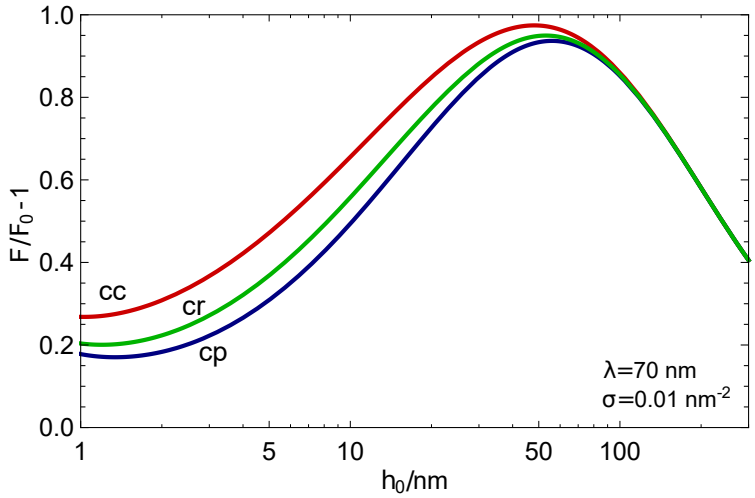

Figure 3.11: Numerical calculation of the electroviscous enhancement of the drag force $F/F_0 - 1$ as a function of h_0, for an initial surface charge density $\sigma = 0.01$ nm^{-2}, and Debye length $\lambda = 70$ nm for constant charge (cc), charge regulation (cr), and constant potential (cp).

With the excess number density $n_m = 2n_0 \cosh(\psi(0)/k_BT)$, one readily finds

$$\Pi = 2n_0 k_B T \left(\cosh \frac{e\psi(0)}{k_B T} - 1 \right). \tag{3.58}$$

The dependence of the osmotic pressure on the film thickness h arises from the midplane potential $\psi(0)$ [59]. At distances h larger than the screening length λ, this potential vanishes, and so does the disjoining pressure.

The repulsive force K between the two surfaces, is obtained as the surface integral the osmotic pressure. The film thickness being much smaller than the curvature radius, we use the Derjaguin approximation [82]. For distances much smaller than the radius of the oscillating sphere, the vertical width of the water film $h = h_0 + R - \sqrt{R^2 - r^2}$ is well approximated by

$$h(r) = h_0 + \frac{r^2}{2R}, \qquad (r \ll R). \tag{3.59}$$

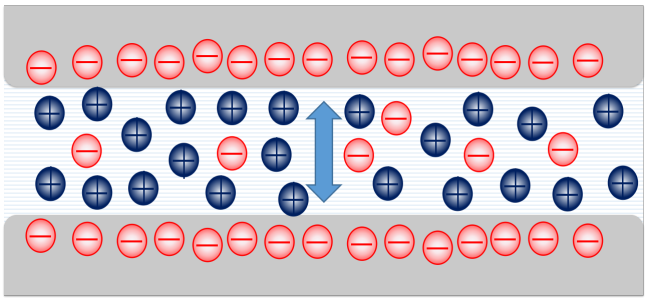

Figure 3.12: .

Rewriting the surface element as $dS = 2\pi drr = 2\pi R dh$, one readily obtains

$$K(h_0) = \int dS\Pi = 2\pi R \int_{h_0}^{\infty} dh\Pi(h). \tag{3.60}$$

Now we consider the repulsive force arising from the overlap of the diffuse layers on the opposite surfaces, and which is independent of the external driving. According to (3.42) the potential at midplane reads as $\psi(0) = (k_B T/e) \ln k$, and the disjoining pressure (3.58) is determined by the parameter k,

$$\Pi = n_0 k_B T \left(k + \frac{1}{k} - 2 \right). \tag{3.61}$$

In Fig. 3.13 we plot Π calculated for constant charge (cc), constant potential (cp), and charge regulation (cr). For distances shorter than the screening length, these different boundary conditions result in significant differences. In agreement with previous work, we find a constant pressure for cp [59] and power laws $\Pi \propto h^s$ with $s = -1$ and $-\frac{1}{2}$ for cc and cr, respectively [83].

The dashed line corresponds to the widely used approximation [84]

$$\Pi_s(h) = 64\beta^2 n_0 k_B T e^{-h/\lambda}, \quad (h \gg \lambda), \tag{3.62}$$

which relies on the linear superposition of the double layers at the opposite surfaces, and where the parameter $\beta = \tanh(e\zeta_\infty/4k_B T)$ is given by the surface potential ζ_∞ at $h_0 \to \infty$,

as defined in eq. (**??**).

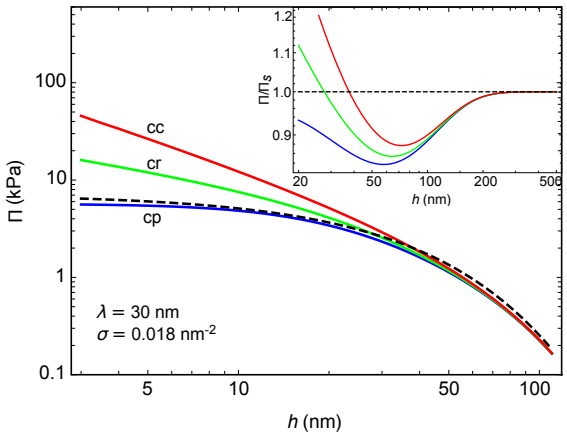

Figure 3.13: Disjoining pressure between charged surfaces as a function of the distance h_0, with screening length $\lambda = 30$ nm. The solid curves give the numerical solution (3.58) for constant surface charge $\sigma = 0.018\text{nm}^{-2}$ (cc), constant potential ζ (cp), and the charge-regulated intermediate case (cr) with dissocation constant $Z = 10^{-3}$M. The approximative expression (4.3) is plotted as dashed line. The inset shows the ratio Π/Π_s, highlighting the deviation of the disjoining pressure Π from the approximate expression Π_s.

The repulsive force (3.60) between the two surfaces is calculated in Derjaguin approximation, in analogy to (**??**), resulting in

$$K = 2\pi R \int_{h_0}^{\infty} dh \Pi(h). \tag{3.63}$$

For the pressure in superposition approximation we obtain $K_s = 2\pi R\lambda\Pi_s(h_0)$ and, after expressing the salt content through the Debye length,

$$K_s = \frac{16R\beta^2 k_B T}{\lambda \ell_B} e^{-h/\lambda}, \qquad (h_0 \gg \lambda). \tag{3.64}$$

A comparison of the numerically exact force K with the exponential approximation K_s is given in Fig. **??**. Both expressions agree beyond 200 nm, or $h_0 > 7\lambda$. Fig. shows the force calculated for constant potential (cp) remains about 10% below K_s, whereas those for constant or regulated charge (cc or cr) show a more complex behavior: they first decrase

below K_s yet at even smaller h_0 by far exceed the analytic approximation K_s [84].

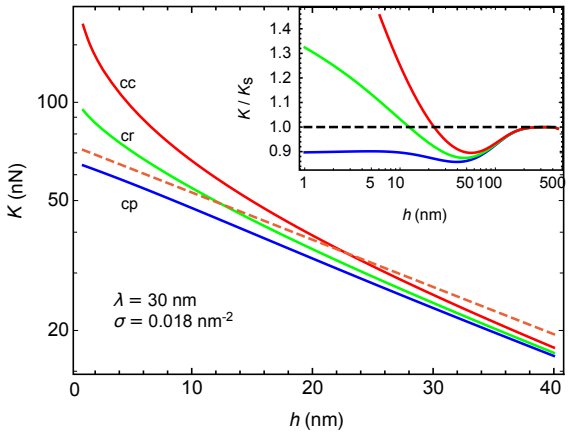

Figure 3.14: Static force between charged surfaces as a function of the distance h_0. The solid curve give the numerical solution (3.60) for constant charge (upper red), constant potential (lower blue), and charge regulation (middle green). The approximative expression (4.7) is plotted as dashed line. The inset shows the ratio K/K_s; note that all curves coincide at large distance, which is not visible in the main figure.

Chapter 4

Disjoining pressure and static repulsion

This chapter aims to investigate some of the basic behavior of an aqueous solution trapped between two charged surfaces, formed by a sphere of radius R and a substrate in a quasistatic state, where the relaxation rate is much larger than the typical oscillation frequencies of the sphere. And to compare the results with previous work relied on the linearization approximation for the hydrodynamic pressure gradient.

Now we consider the static repulsive force arising from the overlap of the diffuse layers on the opposite surfaces, and which is independent of external driving. According to

$$\psi = K_B T/e \left[\ln(m) + 2\ln\left[\mathrm{cd}\left(\frac{z}{2\lambda\sqrt{m}}\middle|m^2\right)\right]\right] \tag{4.1}$$

the potential at z = 0 reads as $\psi(0) = k_B T/e \ln m$, and the disjoining pressure

$$\Pi = n_0 k_B T (m + 1/m - 2) \tag{4.2}$$

is determined by the parameter m,

In Fig. 7 we plot calculated for constant charge (cc), constant potential (cp), and charge regulation (cr). For distances shorter than the screening length, these different boundary conditions result in significant differences. In agreement with previous work, we

find a constant pressure for cp [24] and power laws $\Pi \propto h^s$ with $s = -1$ and $1/2$ for cc and cr, respectively **??**.

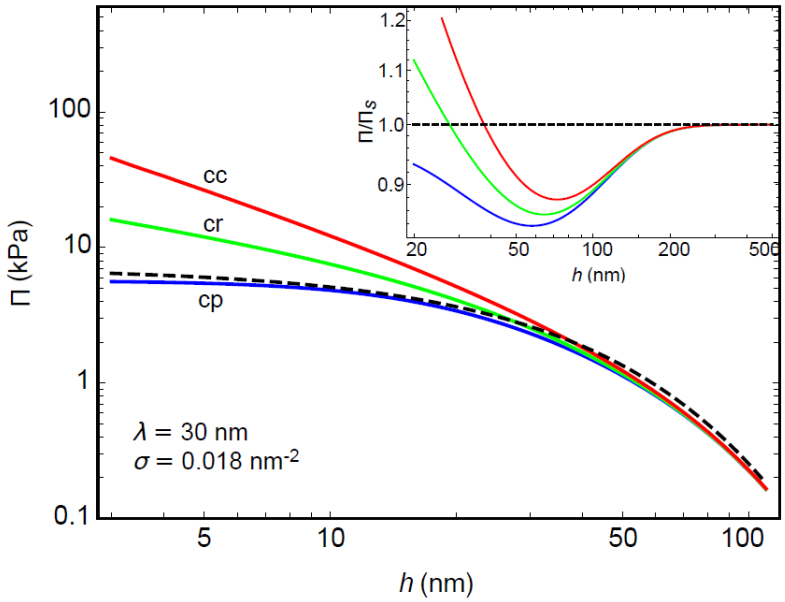

Figure 4.1: Disjoining pressure between charged surfaces as a function of the distance $h_0 4. The solid curves give the numerical solution for constant surface charge 4\sigma = 0.018 nm^{-2}$ (cc), constant potential ζ (cp), and the charge-regulated intermediate case (cr) with a dissociation constant =! $=^{-3}$. The approximative expression is plotted as a dashed line. The inset shows the ratio Π/Π_s, highlighting the deviation of the disjoining pressure Π from the approximate expression Pi_s, which sets in well above 200 nm.

The dashed line corresponds to the widely used approximation [84] which relies on the linear superposition of the double layers at the opposite surfaces, and where the parameter $\beta = \tanh(e\zeta_{\text{inf}}/4k_BT)$ is given by the surface potential ζ_{inf} at h_0 tends to inf.

$$\Pi_s(h) = 64\beta^2 n_0 k_B T e^{-h/\lambda}, \quad (h \gg \lambda), \tag{4.3}$$

which relies on the linear superposition of the double layers at the opposite surfaces, and where the parameter $\beta = \tanh(e\zeta_\infty/4k_BT)$ is given by the surface potential ζ_∞ at

$h_0 \to \infty$, as

$$\beta = \frac{\sqrt{1 + (2\pi\ell_B\lambda\sigma)^2} - 1}{2\pi\ell_B\lambda\sigma} \tag{4.4}$$

The repulsive force (3.60) between the two surfaces is calculated in Derjaguin approximation, in analogy to

$$\xi = \frac{L_{vc}L_{cv}}{L_{vv}L_{cc}} \tag{4.5}$$

resulting in

$$K = 2\pi R \int_{h_0}^{\infty} dh\Pi(h). \tag{4.6}$$

For the pressure in superposition approximation we obtain $K_s = 2\pi R\lambda\Pi_s(h_0)$ and, after expressing the salt content through the Debye length,

$$K_s = \frac{16R\beta^2 k_B T}{\lambda\ell_B} e^{-h/\lambda}, \qquad (h_0 \gg \lambda). \tag{4.7}$$

A comparison of the numerically exact force K with the exponential approximation, K_s is given in Fig. 4.2. Both expressions agree beyond 200 nm, or $h_0 > 7\lambda$. The inset shows that the force calculated for constant potential (cp) remains about 10% below K_s, whereas those for constant or regulated charge (cc or cr) shows a more complex behavior: they first decrease below K_s yet at even smaller h_0 by far exceed the analytic approximation K_s [84].

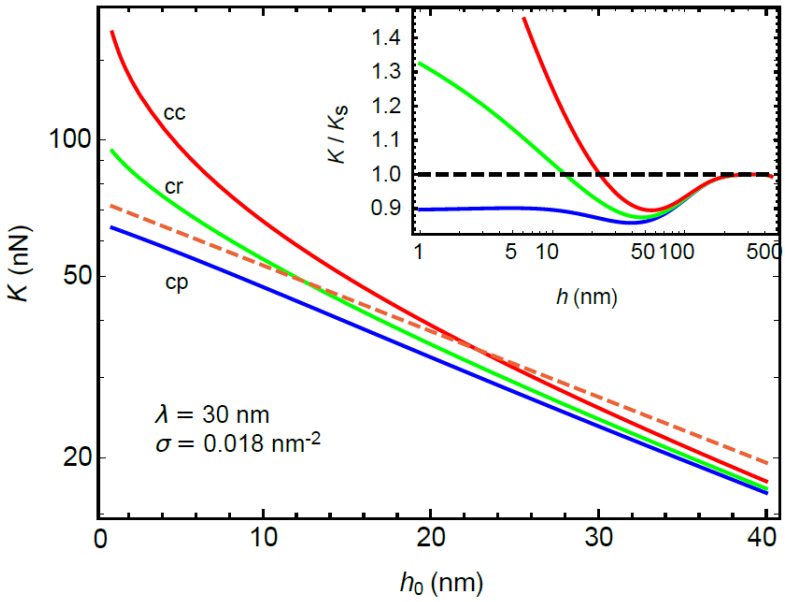

Figure 4.2: Static force between charged surfaces as a function of the distance h_0. The solid curve gives the numerical solution (3.60) for constant charge (upper red), constant potential (lower blue), and charge regulation (middle green). The approximative expression (4.7) is plotted as a dashed line. The inset shows the ratio K/K_s; note that all curves coincide at a large distance, which is not visible in the main figure.

Chapter 5

Viscoelastic effects

So far, we have considered only the electrostatic effect on the system, where the potential ψ is the static equilibrium potential across the channel with screening charges ρ, properties that only vary in the vertical direction. So both the generalized forces $-\nabla P$ and eE are in phase with the velocity. In this section we consider the space charges which develop due to the external drive and that it is characterize by the radial E, $\delta\rho$ and the charge current J_C. As a result of the viscoelastic effect, the trapped fluid experiences a time-dependent stress that translates in a phase shift of the current. We calculate the viscoelastic force using two different approaches, the relaxation time approximation and a series expansion.

From the continuity equation $\partial_t C = D\nabla^2 C - \nabla\cdot J_C$ and the time derivative of Gauss' law it is clear that both J_C and $\nabla\cdot E$ vanish for zero charge modulation, defining $C(r) = \int dz\delta\rho$, and since both vectors have radial components only, we obtain

$$\epsilon\nabla\cdot h\partial_t E = \partial_t C = -\nabla\cdot J_C. \tag{5.1}$$

5.1 Relaxation time approximation

Noting that forces and currents are oscillating functions of zero mean value, it turns convenient to express the time dependence of currents and forces in terms of $X(t) = X_0 e^{i\omega t}$

$$i\omega E = -\frac{1}{h\epsilon} J_C = \frac{e}{h_0 \varepsilon \eta} \left(L_{cv} \nabla P - L_{cc} e E \right). \tag{5.2}$$

where we define the time required for the fluid to recover from the applied stress as

$$\frac{1}{\tau} = \frac{e L_{cc}}{h\varepsilon}, \tag{5.3}$$

Rearranging the terms and solving for E, we find

$$E = \frac{L_{cv}}{L_{cc}} \frac{\nabla P}{1 + i\omega\tau}, \tag{5.4}$$

Inserting the above electric field in the volume current that we previously defined as

$$J_V = -L_{vv} \nabla P + L_{vc} E,$$

and solving for the pressure gradient, we have

$$\nabla P = -\frac{1}{1 - \xi/(1 + i\omega\tau)} \frac{6\eta r V}{h^3}. \tag{5.5}$$

In physical terms the pressure gradient is no longer in phase with the external driving but shows a phase shift $\tan\delta = \omega\tau$. In the quasistatic limit $\omega\tau \ll 1$, we recover the solutions for the electric field

$$E = \frac{L_{cv}}{L_{cc}} \nabla P \tag{5.6}$$

and the pressure gradient

$$\nabla P = -\frac{6\eta r V}{h^3} \frac{1}{1 - \xi} \tag{5.7}$$

at zero charge current.

First approximation

As a first approximation to the problem we solve for the force assuming that both the coupling parameter ξ and the relaxation rate τ are constant with respect to h

$$F = 2\pi \int drrP \tag{5.8}$$

we obtain a first expression for the force

$$F = -\frac{6\pi\eta V R^2}{h_0} \frac{1 - i\omega\tau}{1 - \xi - i\omega\tau} \tag{5.9}$$

We plot in the figure 5.1 the force $F = F_{\mathrm{Re}} + iF_{\mathrm{Im}}$ where its real part describes the viscous drag in phase with the external driving $V(t)$, and the imaginary part the out-of-phase or elastic response for $\omega\tau = 0.5$ and 1.

$$F_{\mathrm{Re}} = -\frac{6\pi\eta V R^2}{h_0} \frac{1 - \xi + (\omega\tau)^2}{(\xi - 1)^2 + (\omega\tau)^2} \quad \text{and} \quad F_{\mathrm{Im}} = \frac{6\pi\eta V R^2}{h_0} \frac{\xi\omega\tau}{(\xi - 1)^2 + (\omega\tau)^2} \tag{5.10}$$

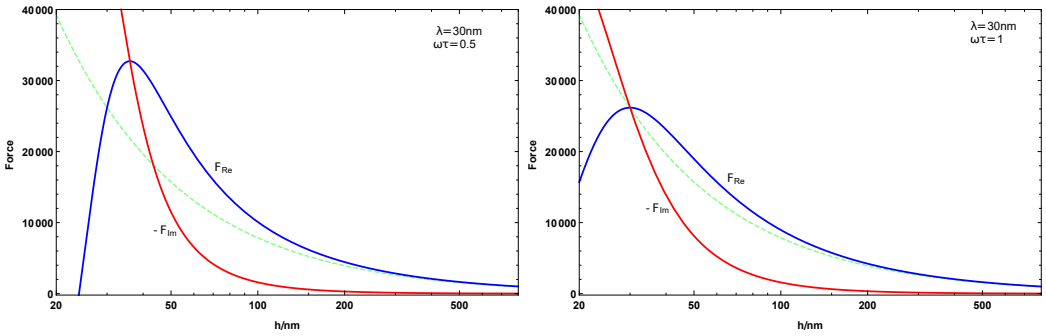

(a) (b)

Figure 5.1: Viscoelastic force as a function of the distance for $\omega\tau = 0.5$ and 1 where the blue line is the real component F_{Re} and the red one $-F_{\mathrm{Im}}$, the green line displays the static case F_0.

Wide channel approximation

By considering a time dependency in the solution for ξ and expanding ∇P in powers of ξ

$$\nabla P = -\nabla P_0 \left(1 + (1 + i\omega\tau)\xi + (1 + 2i\omega\tau - \omega\tau^2)\xi^2 + ...\right) \tag{5.11}$$

and resorting to the wide-channel approximation, meaning using the solution for the correction ξ

$$\xi = \frac{\lambda_*^2}{2h^2}\frac{1}{1+\sigma/h_0 n_0} \qquad \text{with} \qquad \lambda_* = 6\hat{\zeta}\sqrt{\frac{a}{\ell_B}}\lambda, \tag{5.12}$$

when we integrate the hydrodynamic pressure we obtain the complex force

$$\frac{F}{F_0} = 1 + \frac{1}{6}\frac{\lambda_*^2}{h_0^2}\frac{1}{1+i\omega\tau} + ... \tag{5.13}$$

In Fig. 5.2 we plot the variation with distance of the viscoelastic force $F = F_\mathrm{r} + iF_\mathrm{i}$, as calculated from eqs. (5.5) and (5.8) for $\omega\tau = 0.5$ and $\omega\tau = 1$. Comparison with the corresponding curve for the quasi-static case $\omega\tau = 0$ shown in Fig. 3.7, reveals an overall reduction of the electroviscous force at finite frequency, $|F(\omega)| < F(0)$.

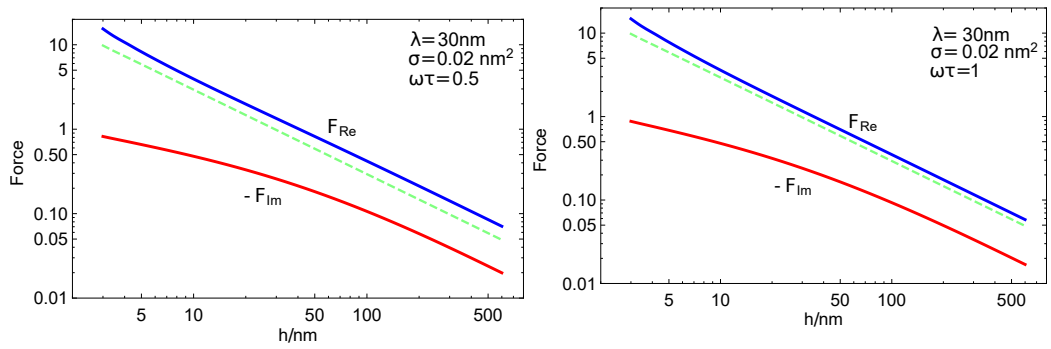

(a) (b)

Figure 5.2: Viscoelastic force as a function of the distance for $\omega\tau = 0.5$ and 1 where the blue line is the real component F_Re and the red one $-F_\mathrm{Im}$, the green line displays the static case F_0.

With the bulk conductivity and a distance h_0 of 100 nm, this rate takes values of the order

$$\frac{1}{\tau} \sim \frac{k_B T}{6\pi\eta h_0 \lambda^2 n_0} \sim 10^5 \mathrm{s}^{-1}. \tag{5.14}$$

This means that the radial charge distribution is achieved on a time scale well below a microsecond, much faster than the oscillations of the cantilever in our AFM experiments.

On the other hand, diffusion of ions over the lubrication length $r_0 = \sqrt{h_0 R}$ occurs on

the time scale $\tau_D = r_0^2/D$. With $h_0 = 100$ nm, $R = 100\mu$m and the diffusion coefficient $D = 10^{-10}\mathrm{m}^2\mathrm{s}^{-1}$, the corresponding rate takes the value $1/\tau_D \sim 10\mathrm{s}^{-1}$, which a posteriori justifies our neglecting diffusion in the charge current (5.2).

Finally we note that the left-hand side of (5.1) relies on the assumption that both the current J_C and the electric field E are confined to the film of thickness h. this is true for J_C because of charge conservation, however the confinement of the electric field, is satisfied only for a vanishing permittivity ϵ_s of the solid surfaces is much smaller than that of water ϵ.

In reality, the permittivity ratio ϵ_s/ϵ is about 1/20 for silica and 1/15 for mica. At radial distances much larger than the thickness h_0, the electric field E penetrates in the solid surfaces, and the left-hand side of (5.1) reads $\epsilon h \nabla \cdot \partial_t E$, rendering the relation between E and J_C significantly more complex. Yet even for zero permittivity contrast, $\epsilon_s = \epsilon$, the finite term on the left-hand side of (5.1) would merely result in a rather insignificant correction factor in the relaxation rate.

Charge conservation

Since the total electric charge in our system never changes, the charge conservation law must be met. Giving the continuity equation between the charge density $\delta\rho$ and the current density J_C

$$\partial_t \delta\rho + \nabla \cdot j = 0 \tag{5.15}$$

And by Gauss's law,

$$\nabla \cdot E = \delta\rho/\varepsilon \tag{5.16}$$

The radial Electric field as well as the charge distribution $\delta\rho(r)$ describe the response to the mechanical driving $V(t) = A\omega\cos(\omega t)$, therefore they oscillate with the frequency ω.

Many electroviscous studies rely on a channel between two electrolyte reservoirs, where

the steady-state is characterized by a constant streaming current $J_C = 0$. Contrary to this open geometry, the squeezing-motion with periodic driving does not allow for a steady current, but requires that a zero mean value, averaged over one period $2\pi/\omega$,

$$\int_0^{2\pi/\omega} dt J_C = 0 \tag{5.17}$$

A total current arises if the streaming and the conduction contributions of $L_{cv}\nabla P$ and $L_{cc}eE$ show a finite phase angle δ

$$J_C \propto \cos(\omega t - \delta) \tag{5.18}$$

That for charge conservation implies that the screening charges density $\delta\rho$

$$\delta\rho \propto \sin(\omega t - \delta) \tag{5.19}$$

The observed phase shift describes the relaxation process, hence it can be expressed as a function of the frequency ω and the characteristic time τ, $\tan(\delta) = \omega\tau$.

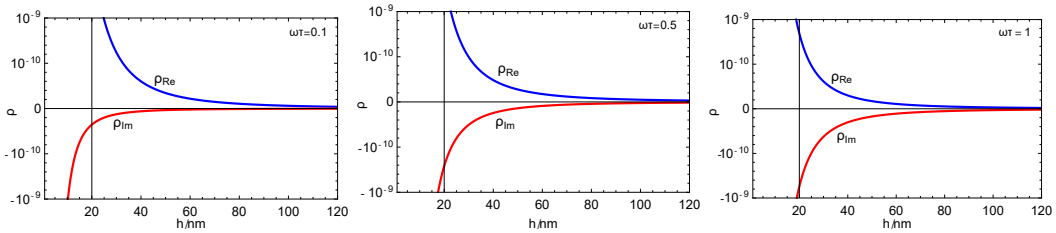

(a) (b) (c)

Figure 5.3: Charge density as a function of the distance for $\lambda = 30$ nm and $\sigma = 0.2\text{nm}^{-2}$ comparing for $\omega\tau = 0.1, 0.5$ and 1 where the blue line is the real component $\delta\rho_{\text{Re}}$ and the red one $\delta\rho_{\text{Im}}$

5.2 Series expansion

We start from the usual pressure for a Poiseuille flow, and we assume that modifications due to charge effects can be cast in the form of a power series in h_0/h,

$$\nabla P = \frac{6\eta r V}{h^3}\left(1 + \sum_{n>3} p_n \left(\frac{h_0}{h}\right)^{n-3}\right). \tag{5.20}$$

Similarly we write the electric field as

$$eE = eE_0 \frac{r}{r_0} \sum_n e_n \left(\frac{h_0}{h}\right)^n, \tag{5.21}$$

where e_n are complex numbers.

Then the volume (J_V) and charge (J_C) flow equations and provide a relation between the coefficients p_n and e_n,

$$p_n = -\frac{\hat{\zeta} h_0}{4\pi \ell_B} \frac{2eE_0}{\eta V r_0} e_{n-2} \qquad (n > 3), \tag{5.22}$$

where $p_3 = 1$. The prefactor on the right hand side compares the electric and viscous forces.

We separate the constant and h-dependent contributions of L_{cc} and L_{cv} according to

$$L_{cc} = L^0_{cc} + L^1_{cc}\frac{h}{h_0}, \quad L_{cv} = L^1_{cv}\frac{h}{h_0}$$

Resulting in a recursion relation for the coefficients e_n,

$$\left(\frac{i\omega h_0 \varepsilon \eta}{e^2} + L^1_{cc}\right) e_n = \frac{12}{h_0^3}(L^1_{cv})^2 e_{n-2} - L^0_{cc} e_{n-1} \tag{5.23}$$

In our system, the pressure gradient will advect the counter-ions in the electrolyte solution that give rise to an electric field generating osmotic flow and electrophoresis. However, before this electric field, the flow of the mobile charges will depend only on the gradient of pressure.

So, in an initial time ($t = 0$) one can express

$$J_C = -L_{cv}\frac{\nabla P}{\eta} \tag{5.24}$$

This simplification applied to equation (5.22) and as an approximation replacing the spatially varying factor h with h_0. Since $p_1 = 0$ and $p_2 = 0$ implies that the first two coefficients of the electric field $e_1 = 0$ and $e_2 = 0$ so the initial point of the system has a solution from $n = 3$ since $p_3 = 1$

In a initial time, when there is not an electric field but only a gradient of pressure, the contribution of the electric field coefficients will be attributed to the advected charges, described by the coefficient L^1_{cv} in the first coefficient, e_{n_0}. The electro-osmotic flow as well as the electrical conductivity are shown and become more important as higher terms solutions are considered and are included in $\tilde{b}$ and $\tilde{a}$.

The total charge of the system can be obtained by integrating the charge density over the surface as

$$c_n = 2\pi \int_0^r dr r \delta\rho = \frac{2eE_0 h_0 n\pi r_0 \varepsilon e_n}{n+1} \tag{5.25}$$

We can see that from the value $n > 3$ the behaviour is always the same. where for the total solution both real and imaginary part are zero, as expected. A more detail calculation can be found in Appendix A.

General solution

As a more general solution, we solve directly for the charge flow

$$\nabla \cdot \partial_t E = i\omega \nabla \cdot E = -\frac{e}{h\varepsilon}\nabla \cdot J_C. \tag{5.26}$$

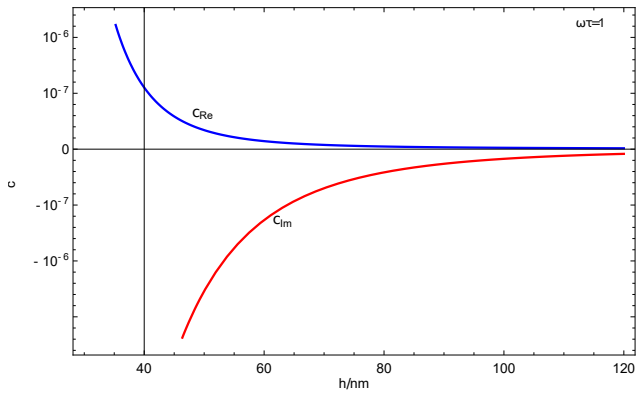

Figure 5.4: Real and Imaginary terms of the charge

Allowing us to express the system as

$$\begin{aligned}\left[E_0 h_0^3 r_0 \left[e^2(hL_{cc}^1(n-1)+h_0 L_{cc}^0 n)-i\omega\varepsilon\eta h_0 hn\right]e_n\right]\left(\frac{h_0}{h}\right)^n \\ = -12ehL_{cv}^1(h(n-2)-h_0(n-1))RV\eta p_n\left(\frac{h_0}{h}\right)^n\end{aligned} \tag{5.27}$$

The total force as a function of the coefficients p_n

$$F = 2\pi\int drrP = \frac{6\pi\eta V R^2}{h_0}\left(1+\sum_{n>3}\frac{2p_n}{(n^2-3n+2)}\right) \tag{5.28}$$

Evaluating the force and adding them, where F_n corresponds to $\sum^n F_n$, we observe for the first 7 solutions, that the force, both in the real as well as the imaginary contribution, it is smaller than when the force is purely due to the osmotic pressure for small distance h_0, and it has a tendency to reach F_3 as h_0 grows.

We can see that from the value $n > 3$, the correction added for the coefficients p_n have a bigger impact in the force for $h_0 \sim 2\lambda$. However, for larger distances, the force will linearly approach Poiseuille flow force. As one can see in the figure 5.5, the frequency has a big influences in the values that can reach by the force when the system is at distances closer to 2λ values, however, the correction for the pressure driven force will decrease faster for larger $\omega\tau$, and the effect will not be noticeable when the distance is increased.

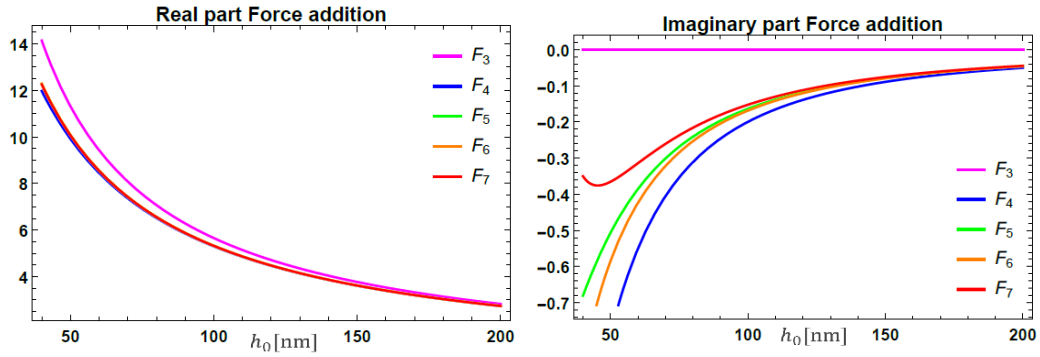

(a) (b)

Figure 5.5: Viscoelastic force as a function of the distance for $\omega\tau = 0.5$ and 1 where the blue line is the real component F_{Re} and the red one $-F_{\mathrm{Im}}$, the green line displays the static case F_0.

5.3 Relaxation Time Approximation vs Series Expansion

The force expression obtained through relaxation approximation and by the series expansion approximation can be expanded as a geometric series, they have the form

$$\frac{F}{F_0} = 1 + \frac{1}{6}\frac{\lambda_*^2}{h_0^2}\frac{1}{1+i\omega\tau} + ... \tag{5.29}$$

Its real part describes the viscous drag in phase with the external driving V (t), and the imaginary part the out-of phase "elastic" response.

Considering that both systems, we can see that for a very small $\omega\tau$ the solution for the force obtained trough the series expansion method approaches the relaxation time approximation in the imaginary contribution, however, for the real part of the solution, include by the relaxation approximation is always larger, since the force obtained by expanding in series terms is always small.

When the frequency ω tends to be small, we recover the static state of the system, when there is no time dependency, this implies that if the sphere is not oscillating, then there wont be a dephasing in the total force, or not a viscous force in the fluid that is being advected.

Chapter 6

Discussion

Validity of the narrow and wide channel approximation

If the double layers on either side of the capillary don't overlap, their properties are given by the Poisson-Boltzmann potential calculated for an infinite half-space.

$$\psi = -\frac{4k_BT}{e}\text{arctanh}(\gamma e^{-z/\lambda}),$$

This approach is widely used to describe electrokinetic and osmotic phenomena in capillaries [3, 34]. Its range of validity is obviously related to the Debye length λ, our analysis shows that in reality it is limited by a significantly larger distance λ_*, as defined in (3.27) which is proportional to the electrokinetic potential. With typical values of the reduced potential $\hat{\zeta}$ ranging from 1 to 4, the parameter λ_* may be up to 20 times larger than the actual screening length λ.

By observing the electroviscous coupling parameter ξ , it can be concluded that an analytical approach to solve the narrow-channel approximation 3.4 provides a good description only for the range where $h_0 \leq \lambda$, whereas the opposite limit 3.3 converges only at $h_0 > 20\lambda$.

Unfortunately it is impossible to obtain the electroviscous drag force from the coupling parameter obtained from a narrow channel approximation

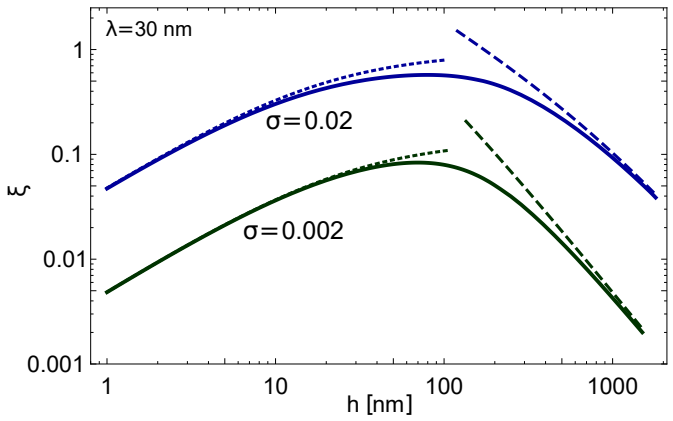

Figure 6.1: Numerical calculation of the electroviscous coupling parameter ξ as a function of h, for surface charge density $\sigma = 0.002$ and $0.02\,\mathrm{nm}^{-2}$, and Debye length $\lambda = 30$. Dotted and dashed lines correspond to the approximations of narrow and wide channels, respectively, whereas the solid lines give the numerical solution.

$$\xi = \frac{\pi\sigma^2 ah}{\pi\sigma^2 ah + 4(\sigma + n_0 h)}.$$

since the excess pressure $P(h) = 6\eta V \int_h^\infty \frac{dh'}{h'^3} \frac{1}{1-\xi(h')}$ is normalized with respect to the equilibrium value at infinity. As a consequence, in the most interesting intermediate range, the force can only be calculated numerically. This can not be overcome by resorting to Debye-Hückel approximation, since in the weak-channel limit its validity is restricted to $2\pi\sigma\lambda\ell_B \ll h_0/\lambda$ [59], which applies to very weakly charged surfaces only.

Comparison with previous work

Electroviscous effects on squeezing motion have been studied in several previous papers [3, 5, 7, 10]. All of these works start, more or less explicitly, from the coupled equation system

$$J_V = -L_{vv}\nabla P + L_{vc}eE$$

$$J_C = -L_{cv}\nabla P + L_{cc}eE$$

considering the volume and charge currents. Yet they use, as an essential difference, the unperturbed pressure gradient $\nabla P_0 = -6\eta r V/h^3$ in J_C instead of ∇P. This perturbative approach corresponds to a linearization of the pressure gradient in the coupling parameter ξ,

$$\nabla P_1 = \nabla P_0(1+\xi), \tag{6.1}$$

instead of the exact expression.

As a consequence, electroviscous effects appear as an additive correction to the unperturbed drag force F_0. Thus the wide-channel force of Bike and Prieve [3] is identical to the first two terms of the solution of the force where a width of the water film is much larger than the Debye length, $h \gg \lambda$

$$\frac{F}{F_0} = 1 + \frac{1}{6}\frac{\lambda_*^2}{h_0^2} + \frac{1}{15}\frac{\lambda_*^4}{h_0^4} + \frac{1}{28}\frac{\lambda_*^6}{h_0^6} + ...$$

although our expression (3.30) corresponds to the full series in λ_*/h_0. Similarly, the numerical calculations of Chun and Ladd [5] and Zhao et al. [10], are done with the linearized pressure gradient P_1.

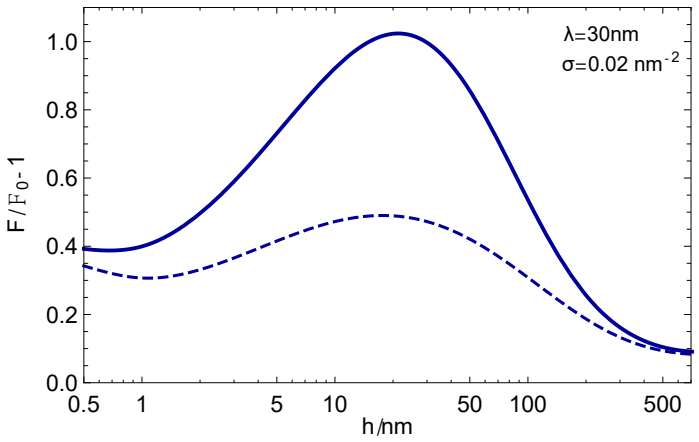

Figure 6.2: Numerical calculation of the electroviscous enhancement of the drag force $F/F_0 - 1$ as a function of h, for $\sigma = 0.02e\,\mathrm{nm}^{-2}$ and $\lambda = 30$ nm. The solid line corresponds to the force calculated numerically with the exact pressure, and the dashed line that with the linearized expression P_1.

In Fig. 6.2 we compare the electroviscous enhancement of the drag force, calculated with the numerically exact pressure gradient

$$\nabla P = -\frac{6\eta r V}{h^3}\frac{1}{1-\xi}$$

and with the linearized form P_1 (6.1). For the parameters $\lambda = 30$ nm and $\sigma = 0.02\,e\,\mathrm{nm}^{-2}$, the linearized force is by about 50% larger than F_0, whereas the increase of the full expression exceeds 100%.

This difference is not surprising in view of the coupling parameters shown in Fig. 6.1 where in the intermediate range where ξ reaches values of the order of unity, one expects a significant nonlinear behavior.

Electroviscous coupling

We calculate the electrostatic and electroviscous properties calculated at constant charge σ as described in section 3.5 (cc) and that of constant potential (cp), where the boundary condition (3.46) is replaced with

$$\psi(\pm h/2) = \zeta_\infty, \tag{6.2}$$

where ζ_∞ is the surface potential at large distance, calculated with the surface charge σ according to (3.43).

In Fig. 6.3 we plot the coupling parameter ξ for the cases of constant charge and constant surface potential, and observe a behavior similar to that of disjoining pressure and repulsive force: At distances beyond the screening length $h > \lambda$, the electrostatic boundary condition is of little relevance, whereas at short distances, $h < \lambda$, both of the curves calculated numerically for constant charge and constant potential diverge.

The electroviscous drag force F depends in a rather intricate manner and non-linear manner on ξ, resulting in a much weaker effect of the electrostatic boundary condition. Indeed, the curves for constant charge and constant potential shown in Fig. 6.4, differ by

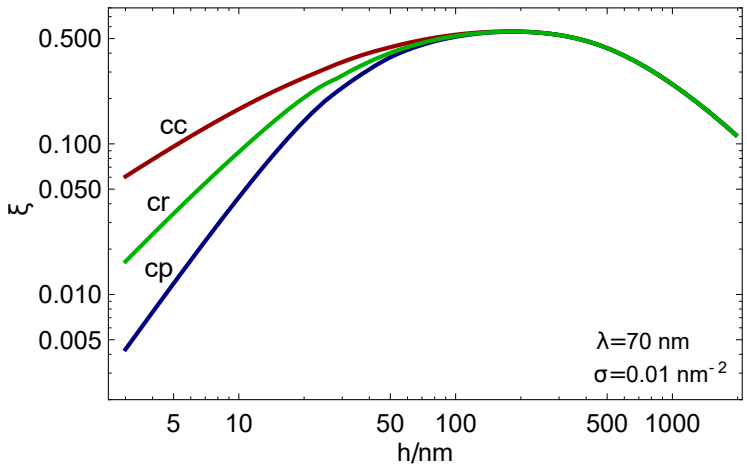

Figure 6.3: Electroviscous coupling parameter ξ as a function of the distance h, for both constant charge (cc), constant potential (cp) and charge regulation (cr).

15%, whereas the corresponding coupling parameters ξ differ by more than one order of magnitude.

Comparison with experiments

In order to verify the validity of our expression we compare with the experimental data obtained by the group of Nano-physics of fluids at interfaces at Laboratoire Ondes et Matiere d'Aquitaine. They performed a dynamic AFM measurement with colloidal probe following the method described in [85]. A spherical particle with a radius of $R = 55 \pm 0.5$ μm was glued at the end of a cantilever. Then mica surface was driven by a piezo to approach the spherical particle with a very small velocity such that the hydrodynamic force can be neglected, and meanwhile the probe was also driven with a base oscillation amplitude $A_\mathrm{b} = 3.5$ nm and frequency of $\omega/2\pi = 100$ Hz. The oscillations of the cantilever with respect to the mica surface causes a Poiseuille flow that depends on time as well as electrokinetic phenomena due to the displacement of charges in the fluid.

They proceed to record the DC component of the cantilever deflection, from which the separation distance h_0 and electrostatic force F between the sphere and the mica surface

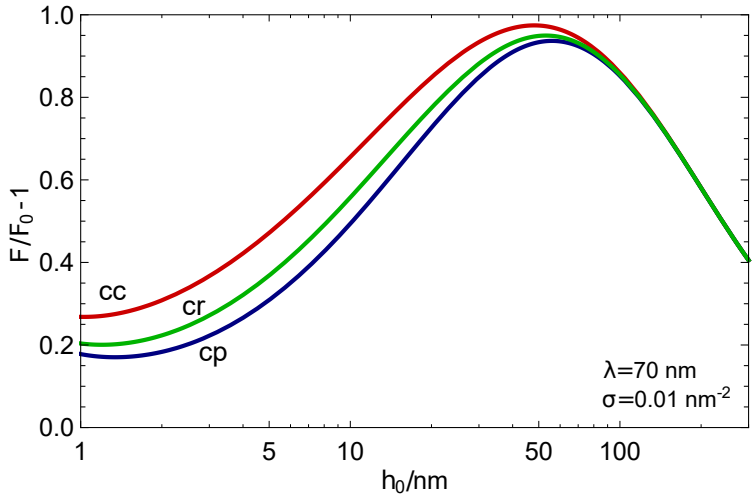

Figure 6.4: Electroviscous drag force F as a function of h_0 for cc, cp and cr boundary conditions.

were extracted. The mica surface and cantilever probe are immersed in the electrolyte solution of 0.1 mM NaCl.

Fig. 6.6 shows the electrostatic force in a weak electrolyte solution, of approximately 0.1 mM NaCl. The upper (red) curve is calculated from the definition of the Static force

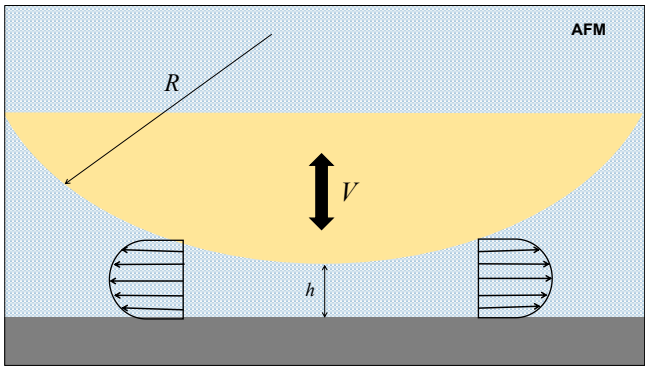

Figure 6.5: Enhancement of the drag force due to electroviscous coupling. The green points are measured AFM data, and the black dots give $F/F_0 - 1$.

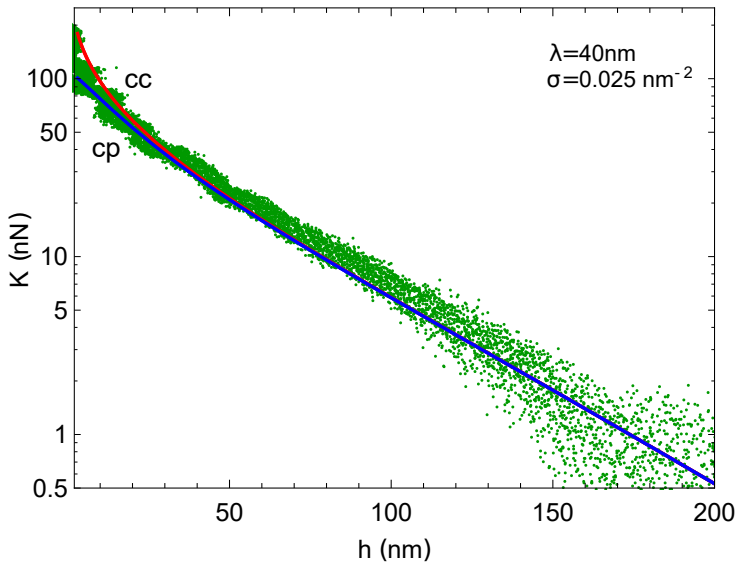

Figure 6.6: Static repulsion K between the AFM sphere and the solid surface, as a function of the distance h_0. The squares give experimental data. The blue and red curves are calculated from (4.6) for constant potential and constant surface charge, respectively, with the parameter values $R = 55\mu$m, surface charge density $\sigma = 0.025\text{nm}^{-2}$ and screening length $\lambda = 40$nm.

$$K = 2\pi R \int_{h_0}^{\infty} dh \Pi(h). \tag{6.3}$$

for constant charge density $\sigma = 0.025\text{nm}-2$, and the lower (blue) one for constant surface potential $\zeta = -95\text{mV}$. Both curves are calculated for a Debye length $\lambda = 40nm$.

Fig. 6.7 we plot the numerical calculation of the electroviscous enhancement of the drag force $F/F_0 - 1$ as a function of h together with the measured the viscous component of the drag force on a 55μm-sphere mounted on an AFM cantilever, as a function of the distance h_0. For a low concentration of the salinity solution, when the distance is large, the elastic component of the force is zero. The fitting is considering Debye length of $\lambda = 40$ nm and a constant charge of $\sigma = 0.008$ nm^{-2}, while the observed Debye length was $\lambda = 28 \pm 2$nm. The fact that the fitting for the smaller values of h could be related to slight deviation of the λ or sigma used for the numerical computation with regard to the measured ones.

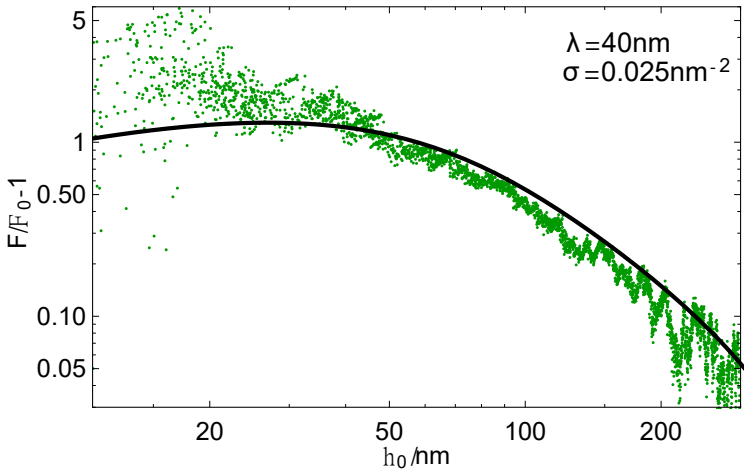

Figure 6.7: Enhancement of the drag force due to electroviscous coupling. The green points are measured AFM data, and the black dots give $F/F_0 - 1$.

Chapter 7

Conclusion

The main aim of the work presented in this thesis was to develop and apply a theoretical model of the dynamic properties of electric double layers in a confined geometry. In particular the properties of confined electrolytes in the nanoscale range in a sphere-plane geometry. We have studied the electroviscous and electrostatic forces exerted on a vibrating AFM tip across a nanoscale water film and compared them with obtained experimental data.

In chapter 3 in the framework of Onsager relations for generalized fluxes and forces, we derive the drag coefficient (**??**) in terms of the electroviscous coupling parameter ξ, and find a quantitative agreement with experimental data (Fig. **??**). As the only parameters, the surface charge σ and the screening length λ are taken from the electrostatic repulsion shown in Fig. 6.6.

This analysis relies on a quasistatic approximation (**??**), where the radial charge distribution in the water film is assumed to follow instantaneously the external driving. The fits of the viscous and elastic components of the response function (**??**), measured at $\omega/2\pi = 100$ Hz and shown in Figs. 3.5 and **??**, indicate that this approximation is justified at distances larger than the screening length, yet ceases to be valid for $h_0 < \lambda$. Our experimental data strongly suggest that in this range both the spring constant k and the drag coefficient γ vary with frequency. The nature of the underlying relaxation process is

not clear at present.

Electroviscous effects on squeezing motion have been studied in several previous papers. All of these works start, more or less explicitly, from the volume and charge currents. Yet when calculating the charge current J_C, they use the unperturbed pressure gradient $\nabla P_0 = -6\eta r V/h^3$ instead of ∇P. This perturbative approach corresponds to a linearization of the pressure gradient in the coupling parameter ξ,

$$\nabla P_1 = \nabla P_0(1-\xi), \tag{7.1}$$

instead of the exact expression. As a consequence, electroviscous effects appear as an additive correction to the unperturbed drag force F0. Thus the wide-channel force of Bike and Prieve is identical to the first two terms of our presented series expansion, whereas our expression corresponds to the full series in λ/h_0. Similarly, the numerical calculations of Chun and Ladd and Zhao et al., are done with the linearized pressure gradient P1. In this work we compare the electroviscous enhancement of the drag force, calculated with the numerically exact pressure gradient and with the linearized form P1. For the parameters $\lambda = 50nm$ and $\sigma = 0.03nm^{-1}$, the linearized drag coefficient (dashed line) is 28% larger than 0, whereas the increase of the full expression (solid line) attains 40%. This difference is not surprising in view of the coupling parameters; in the intermediate range where ξ reaches values of the order of unity, one expects a significant nonlinear behavior.

Charge regulation turns out to be of minor importance in the experimentally most relevant range. Indeed, the electroviscous coupling sets in at large distances and is maximum at $h_0 \sim 3\lambda$ (Fig. **??**), whereas the electrostatic boundary conditions and charge regulation effects are significant in narrow channels only, as shown in Figs. 6.3–6.6.

Appendix A

Series expansion

We start from the usual pressure for a Poiseuille flow, and we assume that modifications due to charge effects can be cast in the form of a power series in h_0/h,

$$\nabla P = \frac{6\eta r V}{h^3}\left(1 + \sum_{n>3} p_n \left(\frac{h_0}{h}\right)^{n-3}\right). \tag{A.1}$$

Similarly we write the electric field as

$$eE = eE_0 \frac{r}{r_0} \sum_n e_n \left(\frac{h_0}{h}\right)^n, \tag{A.2}$$

where e_n are complex numbers.

To make a general review, it is necessary to recall that the diffusion of the advected counter-ions occurs on a time scale $\tau_D = Rh_0/D$, of the order of a second, which turns out to be much larger than the time scale arising from the coupled currents. Thus we discard the diffusion term $D\nabla^2 C$ in

$$\partial_t C = D\nabla^2 C - \nabla \cdot J_C, \tag{A.3}$$

and using Gauss' law, we rewrite $\partial_t C$ as the time derivative of $\partial_t C = \nabla \cdot E$, resulting in

$$\nabla \cdot \partial_t E = i\omega \nabla \cdot E = -\frac{e}{h\varepsilon} \nabla \cdot J_C. \tag{A.4}$$

In order to recover a homogeneous expression in powers of h, we resort to the approximation

$$i\omega E = -\frac{e}{h\varepsilon} J_C. \tag{A.5}$$

This simplification applied to equation (5.22) and as an approximation replacing the spatially varying factor h with h_0. Since $p_1 = 0$ and $p_2 = 0$ implies that the first two coefficients of the electric field $e_1 = 0$ and $e_2 = 0$ so the initial point of the system has a solution from $n = 3$ since $p_3 = 1$

We separate the constant and h-dependent contributions of L_{cc} and L_{cv} according to

$$L_{cc} = L^0_{cc} + L^1_{cc}\frac{h}{h_0}, \quad L_{cv} = L^1_{cv}\frac{h}{h_0}$$

Inserting the above expressions we find relation for the coefficients p_n and e_n,

$$L^1_{cv}\frac{6\eta r V}{h_0^3} p_n = eE_0\frac{r}{r_0}\left[\left(\frac{i\omega h_0 \varepsilon \eta}{e^2} + L^1_{cc}\right) e_n + L^0_{cc} e_{n-1}\right] \tag{A.6}$$

For $n = 3$, we have with p_3

$$\frac{6\eta r_0 V}{eE_0 h_0^3} L^1_{cv} = \left(\frac{i\omega h_0 \varepsilon \eta}{e^2} + L^1_{cc}\right) e_3 + L^0_{cc} e_2 \tag{A.7}$$

For $n > 3$, the pressure coefficient is related to e_n by (5.22), resulting in a recursion relation for the coefficients e_n,

$$\left(\frac{i\omega h_0 \varepsilon \eta}{e^2} + L^1_{cc}\right) e_n = \frac{12}{h_0^3}(L^1_{cv})^2 e_{n-2} - L^0_{cc} e_{n-1} \tag{A.8}$$

We can re-express this equation as

$$e_n = \tilde{a} e_{n-2} - \tilde{b} e_{n-1} \tag{A.9}$$

Where

$$\tilde{a} = \frac{(L^1_{cv})^2}{L^1_{vv}L^1_{cc}}\frac{1}{i\omega\tau+1} \quad \tilde{b} = \frac{L^0_{cc}}{L^1_{cc}}\frac{1}{i\omega\tau+1} \quad \text{and} \quad \frac{1}{\tilde{\tau}} = \frac{h_0\varepsilon\eta}{e^2L^1_{cc}} \tag{A.10}$$

The coefficient $\tilde{a}$ is very close to the definition of ξ while it considered exclusively the effects of the bulk charge. One can see that $\tilde{a} \ll 1$. On the other hand, the second coefficient $\tilde{b}$ includes only the surface density interaction, which leads to $\tilde{a} < \tilde{b}$.

Since $p_1 = 0$ and $p_2 = 0$ implies that the first two coefficients of the electric field $e_1 = 0$ and $e_2 = 0$ so the initial point of the system has a solution from $n = 3$ since $p_3 = 1$

$$e_{n_0} = -i\frac{6Vr_0eh_0^2}{\omega E_0\varepsilon}L^1_{cv} = -i\xi_0 \tag{A.11}$$

Using the notation $e_{n_0} = e_3$ since e_3 is the first solution different to zero. So going back to the main electric field expression (A.9) we get

$$\begin{aligned} e_{n_0+1} &= i\tilde{b}\xi_0 \\ e_{n_0+2} &= -i(\tilde{a}+\tilde{b}^2)\xi_0 \\ e_{n_0+3} &= i(2\tilde{a}+\tilde{b}^2)\tilde{b}\xi_0 \\ e_{n_0+4} &= -i(\tilde{a}^2+3\tilde{a}\tilde{b}^2+\tilde{b}^4)\xi_0 \end{aligned} \tag{A.12}$$

The rest of the coefficients will be also a function of e_{n_0} and depending if the coefficient is an even or odd number.

$$e_{n_0} = -i\frac{6Vr_0eh_0^2}{\omega E_0\varepsilon}L^1_{cv} = -i\xi_0 \tag{A.13}$$

For m even

$$e_{n_0+m_{even}} = -i\upsilon_m\xi_0 \tag{A.14}$$

For m odd

$$e_{n_0+m_{odd}} = i\chi_m\tilde{b}\xi_0 \tag{A.15}$$

Where the coefficients υ_m and χ_m are polynomials of a and b. All coefficients where m is an even number will be negative while for m odd they are positive therms.

We can solve for the pressure also by substituting (**??**) in equation (5.22). The first thing we notice is that the term $p_4 = 0$ since $e_2 = 0$. For the rest of the coefficients the solution follows the same form as the electric field ones; so defining a new constant from p_5

$$p_5 = -\frac{\hat{\zeta} h_0}{4\pi \ell_B} \frac{2eE_0}{\eta V r_0} e_{n_0} = -i \frac{12 e^2 h_0^2}{\omega \eta \varepsilon} (L^1_{cv})^2 = -i\varrho_0 \tag{A.16}$$

As it follows for the rest

$$\begin{aligned} p_6 &= i\tilde{b}\varrho_0 \\ p_7 &= -i(\tilde{a} + \tilde{b}^2)\varrho_0 \\ p_8 &= i(2\tilde{a} + \tilde{b}^2)\tilde{b}\varrho_0 \\ p_9 &= -i(\tilde{a}^2 + 3\tilde{a}\tilde{b}^2 + \tilde{b}^4)\varrho_0 \end{aligned} \tag{A.17}$$

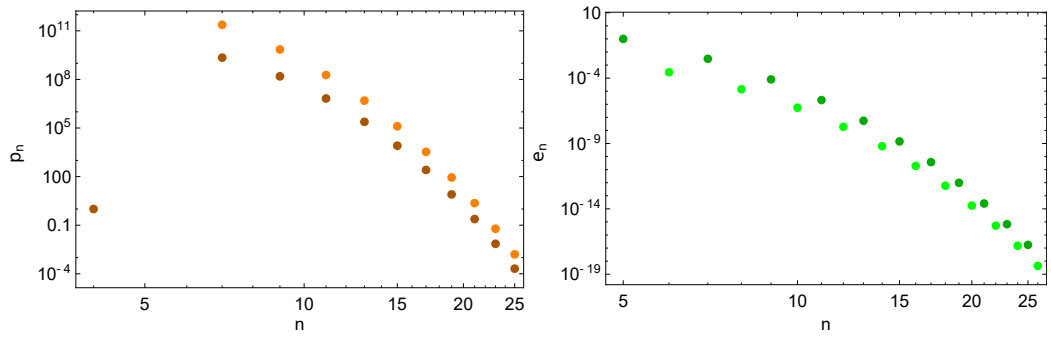

(a) (b)

Figure A.1: Coefficients p_n and e_n.

An we can conclude as well that

$$p_{n_{odd}} = -i\upsilon_m \varrho_0 \quad \text{and} \quad p_{n_{even}} = i\chi_m \tilde{b}\varrho_0 \tag{A.18}$$

For this first approximation and applying the continuity equation

$$\partial_t C = -\nabla \cdot J_C \tag{A.19}$$

We can obtain the charge density terms for different values of n, as expected C_1 and C_2 are zero and we find

$$\begin{aligned}
C_3 &= i\frac{VL^1_{cv}}{100Rh^3}(r^2 - 2h_0R) \\
C_4 &= 0 \\
C_5 &= \frac{VL^1_{cv}}{100Rh^5}(r^2 - 2h_0R)h_0^2\varrho_0 \\
C_6 &= \frac{VL^1_{cv}}{100Rh^6}(r^2 - 2h_0R)h_0^3\tilde{b}\varrho_0 \\
C_6 &= \frac{VL^1_{cv}}{100Rh^7}(r^2 - 2h_0R)h_0^4(\tilde{a} + \tilde{b}^2)\varrho_0
\end{aligned} \tag{A.20}$$

As the charge density depends on both $\tilde{a}$ and $\tilde{b}$, it will have a imaginary and a real contribution.

It is important to notice that for a bigger n the values of both real and imaginary charge density tend to zero and the more relevant coefficient is C_5. And by solving for the charge integrating

$$c = -\int r\nabla \cdot J_C dr \tag{A.21}$$

$$
\begin{aligned}
c_3 &= i\frac{3VL^1_{cv}r^2}{50Rh^2} \\
c_4 &= 0 \\
c_5 &= \frac{3VL^1_{cv}r^2}{50Rh^4}h_0^2\varrho_0 \\
c_6 &= \frac{3VL^1_{cv}r^2}{50Rh^5}h_0^3\tilde{b}\varrho_0 \\
c_6 &= \frac{3VL^1_{cv}r^2}{50Rh^6}h_0^4(\tilde{a}+\tilde{b}^2)\varrho_0
\end{aligned}
\tag{A.22}
$$

The charge is not conserved this case because the initial assumption that $J_C = -L_{cv}\nabla P$ does not considers the total effect of the electric field, since the real part of the coefficient cn_5 and the imaginary part of cn_6 are still relevant, so as making the addition of all the charges as our initial definition of the electric field for larger values of n we get that the total charge is of roughly $c \approx Re(cn_5) + iIm(cn_6)$.

However, as soon as the total definition of the charge flow J_C then the charge in the system is almost conserved.

$$
\begin{aligned}
c_3 &= i\frac{3VL^1_{cv}r^2}{50Rh^2} \\
c_4 &= 0 \\
c_5 &= \frac{3VL^1_{cv}r^2}{50Rh^4}h_0^2\varrho_0 \\
c_6 &= \frac{3VL^1_{cv}r^2}{50Rh^5}h_0^3\tilde{b}\varrho_0 \\
c_6 &= \frac{3VL^1_{cv}r^2}{50Rh^6}h_0^4(\tilde{a}+\tilde{b}^2)\varrho_0
\end{aligned}
\tag{A.23}
$$

We can observe the same behaviour that in the previous case where the coefficients cn_5 and cn_6 have a highest contribution to the charge values, but that are closer to zero since both of them are $\ll 1$

The charge is now conserved this case because the initial assumption that $JC =$

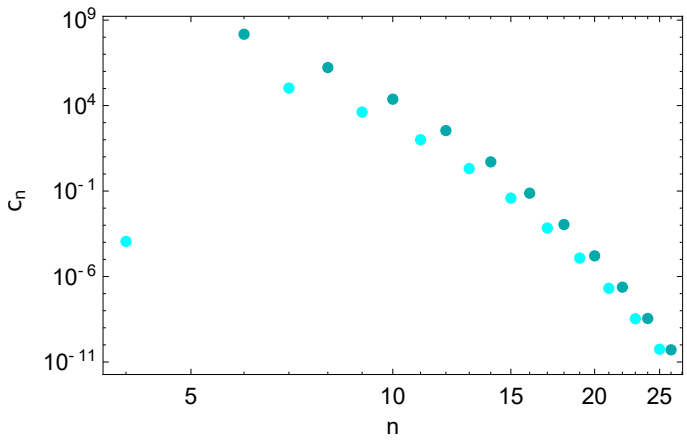

Figure A.2: Real and Imaginary charge coefficients c_n that decrease when the polynomial degree n

$Lcv\nabla P - L_{cc}eE$ does considers the total effect of the electric field, since the real part of the coefficient cn_5 and the imaginary part of cn_6 are still relevant, so as making the addition of all the charges as our initial definition of the electric field for larger values of n we get that the total charge is of roughly $c =\propto \mathrm{Re}(cn_5) + i\mathrm{Im}(cn_6)$. But the solution for the total charge in the total system, after the overall integral in the areal, it is closer to zero even for the larger coefficients found before, since they might be proportional to J_C which by definition is initially zero, then the largest contribution will be proportional to $-iJ_C(n)\omega/r$ for $n > 3$

$$c_n = -i\frac{J_C(n)\omega}{r} \tag{A.24}$$

Solution without approximation

We know from the volume conservation that we can express

$$p_n = \chi e_{n-2} \tag{A.25}$$

and by combining Gauss' law and charge conservation

$$ap_n - be_{n-1} = e_n \tag{A.26}$$

Where

$$\chi = -\frac{\hat{\zeta}h_0}{4\pi l_B}\frac{2eE_0}{\eta V r_0} \quad a = \frac{L^1_{cv}}{L^1_{cc}}\frac{6\eta r_0 V}{h_0^3}\frac{1}{i\omega\tau_D + 1} \quad \text{and} \quad b = \frac{L^0_{cc}}{L^1_{cc}}\frac{1}{i\omega\tau_D + 1} \tag{A.27}$$

This give us the general solution for both e_n and p_n

$$\begin{aligned} e_n =& \frac{1}{2^{n+1}a\chi^2\sqrt{b^2+4a\chi}}\left(b\sqrt{b^2+4a\chi} - b^2 - 2a\chi\right)\left(-b - \sqrt{b^2+4a\chi}\right)^n + ... \\ & \left(b\sqrt{b^2+4a\chi} + b^2 + 2a\chi\right)\left(-b + \sqrt{b^2+4a\chi}\right)^n \end{aligned} \tag{A.28}$$

And

$$\begin{aligned} p_n =& \frac{1}{2^{n+1}a\chi^2\sqrt{b^2+4a\chi}}\left(\left(b^3+2ab\chi\right)\sqrt{b^2+4a\chi} - b^4 - 4ab^\chi - 2a^2\chi^2\right)... \\ & \left(\left(b^3+2ab\chi\right)\sqrt{b^2+4a\chi} + b^4 + 4ab^\chi + 2a^2\chi^2\right) \end{aligned} \tag{A.29}$$

For the first 10 coefficients we get

n	p_n	e_n
3	1	a
4	0	$-ab$
5	$a\chi$	$a(b^2 + a\chi)$
6	$-ab\chi$	$-a(b^3 + 2ab\chi)$
7	$a\chi(b^2 + a\chi)$	$a(b^4 + 3ab^2\chi + a^2\chi^2)$
8	$-a\chi(b^3 + 2ab\chi)$	$-ab(b^2 + a\chi)(b^2 + 3a\chi)$
9	$a\chi(b^4 + 3ab^2\chi + a^2\chi^2)$	$a(b^6 + 5ab^4\chi + 6a^2b^2\chi^2 + a^3\chi^3)$
10	$-ab\chi(b^2 + a\chi)(b^2 + 3a\chi)$	$-ab(b^2 + 2a\chi)(b^4 + 4ab^2\chi + 2a^2\chi^2)$

The charge density of the system is a property that can be known through the definitions of the charge conservation or the Gauss' law since:

$$\partial_t\rho(r) = \nabla \cdot J_C \quad \text{and} \quad \rho = \varepsilon h \nabla E \tag{A.30}$$

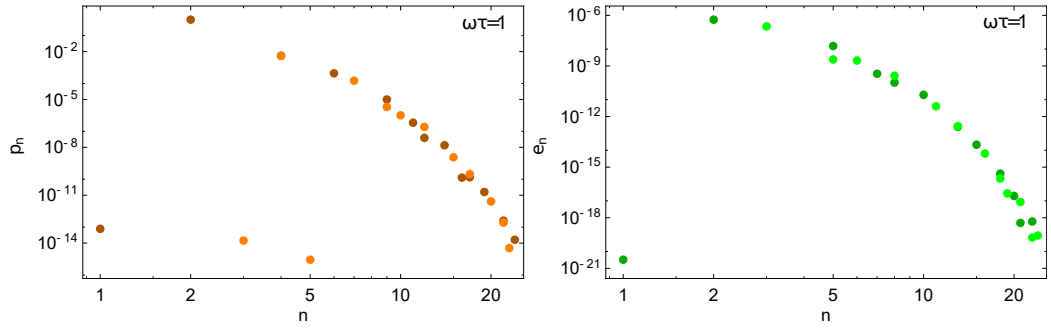

(a) (b)

Figure A.3: Viscoelastic force as a function of the distance for $\omega\tau = 0.5$ and 1 where the blue line is the real component F_{Re} and the red one $-F_{\mathrm{Im}}$, the green line displays the static case F_0.

both solutions are function of n and h_0; from the charge flow J_C

$$\rho(r,n,h_0) = -\frac{i2^{n+1}(neE_0h_0^3L_{cc}Rr_0e_n + 3L_{cv}^1((n-2)r^2 - 2h_0R)(r^2+2h_0R)V\eta p_n)}{h_0^2(r^2+2h_0R)^2}\ldots \left(\frac{h_0R}{r^2+2h_0R}\right)^{n-1} \tag{A.31}$$

The total charge of the system can be obtained by integrating the charge density over the surface as

$$c_n = 2\pi\int_0^r drr\rho \tag{A.32}$$

And we find that from charge conservation

$$c_n = -\frac{21eE_0L_{cc}\pi r_0e_n}{\omega} \tag{A.33}$$

Plotting for the real and imaginary part of both solutions we find

and from Gauss' law

$$\rho = -\frac{2^neE_0nr_0\varepsilon e_n}{R}\left(\frac{h_0R}{r^2+2h_0r}\right)^n \tag{A.34}$$

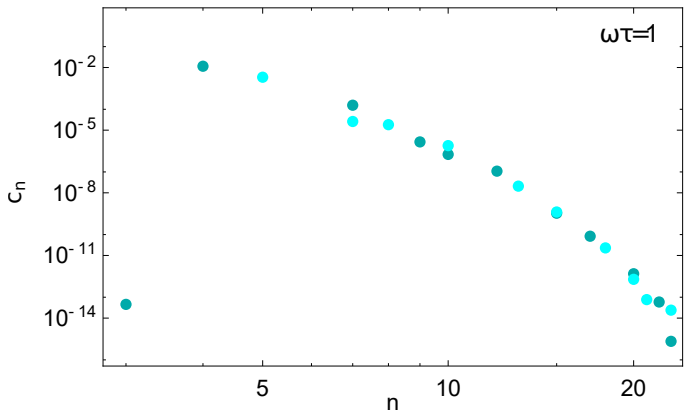

Figure A.4: Caption

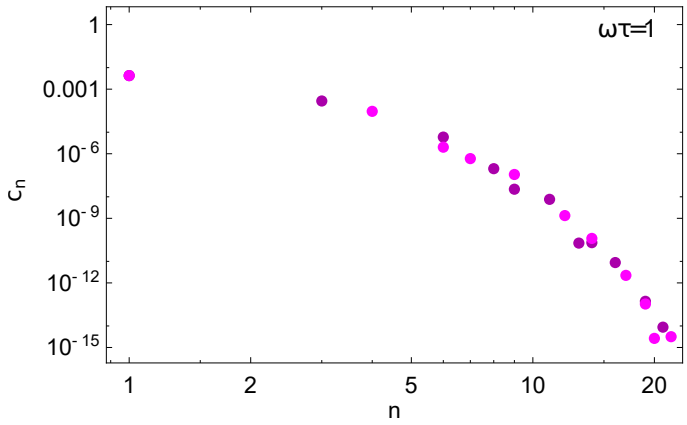

Figure A.5:

Where the total charge

$$c_n = \frac{2eE_0h_0n\pi r_0\varepsilon e_n}{n+1} \tag{A.35}$$

Comparing this two forms of the charge density for different values of n

Solution without approximation

By solving directly from

$$\nabla \cdot \partial_t E = i\omega \nabla \cdot E = -\frac{e}{h\varepsilon}\nabla \cdot J_C. \tag{A.36}$$

Without making the approximation that leads to a general expression

$$\begin{aligned}\left[E_0 h_0^3 r_0 \left[e^2(hL_{cc}^1(n-1)+h_0 L_{cc}^0 n)-i\omega\varepsilon\eta h_0 hn\right]e_n\right]\left(\frac{h_0}{h}\right)^n \\ = -12ehL_{cv}^1(h(n-2)-h_0(n-1))RV\eta p_n\left(\frac{h_0}{h}\right)^n\end{aligned} \tag{A.37}$$

As before we can separate the constants and h-dependent contributions and we rewrite the derivative of h as

$$h'(r) = \frac{2(h-h_0)}{r} \tag{A.38}$$

We know from the volume conservation that we can express

$$p_n = de_{n-2} \tag{A.39}$$

where

$$d = -\frac{\hat{\zeta}h_0}{4\pi\ell_B}\frac{2eE_0}{\eta V r_0} \tag{A.40}$$

That leads to a recursive system for the coefficients p_n, and by combining Gauss' law and charge conservation

$$\begin{aligned}p_{n+2} &= \frac{1}{1-i\omega\tau\frac{n}{n-1}}\left(\left[\frac{2(L_{cv}^1)^2}{L_{vv}^1 L_{cc}^1}-\frac{L_{cc}^0}{L_{cc}^1}\right]p_{n+1}-\frac{2(L_{cv}^1)^2}{L_{vv}^1 L_{cc}^1}p_n\right) \\ &= \frac{1}{1-i\omega\tau\frac{n}{n-1}}\left(\left[2\xi^1-\frac{L_{cc}^0}{L_{cc}^1}\right]p_{n+1}-2\xi^1 p_n\right)\end{aligned} \tag{A.41}$$

Where we apply the definition of ξ as a function of h_0 as

$$\xi^1 = \frac{(L_{cv}^1)^2}{L_{vv}^1 L_{cc}^1} \tag{A.42}$$

To simplify

$$p_{n+2} = a(bp_{n+1}-cp_n) \tag{A.43}$$

Where

$$\begin{aligned} a &= \frac{1}{1 - i\omega\tau\frac{n}{n-1}} \\ b &= \frac{24(L^1_{cv})^2}{h_0^3 L^1_{cc}} - \frac{L^0_{cc}}{L^1_{cc}} \\ c &= \frac{24(L^1_{cv})^2}{h_0^3 L^1_{cc}} \end{aligned} \tag{A.44}$$

Where the definition of the decaying time is

$$\tau_D = \frac{h_0 \varepsilon \eta}{e^2 L^1_{cc}} \tag{A.45}$$

For the first 7 coefficients we get

n	p_n
2	0
3	1
4	ab
5	$a(ab^2 - c)$
6	$a^2 b(ab^2 - 2c)$
7	$a^2(a^2 b^4 - 3ab^2 c + c^2)$
8	$a^3 b(ab^2 - 3c)(ab^2 - c)$

Evaluating the real and imaginary part of the coefficients e_n and P_n they describe an oscillatory behaviour, which is more notorious for a small frequency, since it decays faster to zero when $\omega\tau$ grows.

From the original definition the coefficient $p_3 = 1$ and is from the coefficient p_4 that the viscous effects become relevant (imaginary part of the force). However, the absolute value of the coefficients as a function of the distance h_0 show that contribution of the extra terms tend to zero when the distance is increased.

The total charge of the system can be obtained by integrating the charge density over the surface as

$$Q = 2\pi \int_0^r dr r \rho \tag{A.46}$$

And we find that from charge conservation

$$Q = -\frac{2ieE_0(L_{cc}^0 + L_{cc}^1)\pi r_0 e_n}{\omega} \tag{A.47}$$

And from Gauss' law

$$Q = -\frac{2E_0 h_0 n\pi r_0 \varepsilon e_n}{n-1} \tag{A.48}$$

Bibliography

[1] E. Verwey, "The electrical double layer and the stability of lyophobic colloids.," *Chemical Reviews*, vol. 16, no. 3, pp. 363–415, 1935.

[2] R. J. Gross and J. F. Osterle, "Membrane transport characteristics of ultrafine capillaries," *The Journal of Chemical Physics*, vol. 49, no. 1, pp. 228–234, 1968.

[3] S. G. Bike and D. C. Prieve, "Electrohydrodynamic lubrication with thin double layers," *Journal of colloid and interface science*, vol. 136, no. 1, pp. 95–112, 1990.

[4] J. Lyklema, *Fundamentals of Interface and Colloid Science*. New York: Academic Press, 1995.

[5] B. Chun and A. Ladd, "The electroviscous force between charged particles: beyond the thin-double-layer approximation," *Journal of Colloid and Interface Science*, vol. 274, no. 2, pp. 687–694, 2004.

[6] O. Manor, I. U. Vakarelski, X. Tang, S. J. O'Shea, G. W. Stevens, F. Grieser, R. R. Dagastine, and D. Y. Chan, "Hydrodynamic boundary conditions and dynamic forces between bubbles and surfaces," *Physical review letters*, vol. 101, no. 2, p. 024501, 2008.

[7] F. Liu, A. Klaassen, C. Zhao, F. Mugele, and D. van den Ende, "Electroviscous dissipation in aqueous electrolyte films with overlapping electric double layers," *The Journal of Physical Chemistry B*, vol. 122, no. 2, pp. 933–946, 2018. PMID: 28976197.

[8] D. Stein, M. Kruithof, and C. Dekker, "Surface-charge-governed ion transport in nanofluidic channels," *Physical Review Letters*, vol. 93, no. 3, p. 035901, 2004.

[9] A. M. Smith, A. A. Lee, and S. Perkin, "The electrostatic screening length in concentrated electrolytes increases with concentration," *The journal of physical chemistry letters*, vol. 7, no. 12, pp. 2157–2163, 2016.

[10] C. Zhao, W. Zhang, D. van den Ende, and F. Mugele, "Electroviscous effects on the squeezing flow of thin electrolyte solution films," *Journal of Fluid Mechanics*, vol. 888, p. A29, 2020.

[11] H. A. Stone, A. D. Stroock, and A. Ajdari, "Engineering flows in small devices: microfluidics toward a lab-on-a-chip," *Annu. Rev. Fluid Mech.*, vol. 36, pp. 381–411, 2004.

[12] L. Bocquet and E. Charlaix, "Nanofluidics, from bulk to interfaces," *Chemical Society Reviews*, vol. 39, no. 3, pp. 1073–1095, 2010.

[13] V. M. Aguilella and A. Alcaraz, "Nanobiotechnology: A fluid approach to simple circuits," *Nature nanotechnology*, vol. 4, no. 7, p. 403, 2009.

[14] W. Guan, R. Fan, and M. A. Reed, "Field-effect reconfigurable nanofluidic ionic diodes," *Nature communications*, vol. 2, p. 506, 2011.

[15] J. Clarke, H.-C. Wu, L. Jayasinghe, A. Patel, S. Reid, and H. Bayley, "Continuous base identification for single-molecule nanopore dna sequencing," *Nature nanotechnology*, vol. 4, no. 4, p. 265, 2009.

[16] P. Cadinu, G. Campolo, S. Pud, W. Yang, J. B. Edel, C. Dekker, and A. P. Ivanov, "Double barrel nanopores as a new tool for controlling single-molecule transport," *Nano letters*, vol. 18, no. 4, pp. 2738–2745, 2018.

[17] J. Yan, M. Han, J. Zhang, C. Xu, E. Luijten, and S. Granick, "Reconfiguring active particles by electrostatic imbalance," *Nature materials*, vol. 15, no. 10, pp. 1095–1099, 2016.

[18] R. Capozza, A. Vanossi, A. Benassi, and E. Tosatti, "Squeezout phenomena and boundary layer formation of a model ionic liquid under confinement and charging," *The Journal of chemical physics*, vol. 142, no. 6, p. 064707, 2015.

[19] A. M. Smith, K. R. Lovelock, N. N. Gosvami, T. Welton, and S. Perkin, "Quantized friction across ionic liquid thin films," *Physical Chemistry Chemical Physics*, vol. 15, no. 37, pp. 15317–15320, 2013.

[20] S. McLaughlin, "Electrostatic potentials at membrane-solution interfaces," in *Current topics in membranes and transport*, vol. 9, pp. 71–144, Elsevier, 1977.

[21] H.-J. Butt, "Measuring electrostatic, van der waals, and hydration forces in electrolyte solutions with an atomic force microscope," *Biophysical journal*, vol. 60, no. 6, pp. 1438–1444, 1991.

[22] S. H. Behrens and D. G. Grier, "The charge of glass and silica surfaces," *The Journal of Chemical Physics*, vol. 115, no. 14, pp. 6716–6721, 2001.

[23] M. Elimelech, J. Gregory, X. Jia, and R. Williams, "Chapter 2 - electrical properties of interfaces," in *Particle Deposition & Aggregation* (M. Elimelech, J. Gregory, X. Jia, and R. Williams, eds.), pp. 9–32, Woburn: Butterworth-Heinemann, 1995.

[24] A. K. Kulshreshtha, O. N. Singh, and G. M. Wall, *Pharmaceutical suspensions: from formulation development to manufacturing*. Springer, 2009.

[25] I. Brigger, L. Armand-Lefevre, P. Chaminade, M. Besnard, Y. Rigaldie, A. Largeteau, A. Andremont, L. Grislain, G. Demazeau, and P. Couvreur, "The stenlying effect of high hydrostatic pressure on thermally and hydrolytically labile nanosized carriers," *Pharmaceutical research*, vol. 20, no. 4, pp. 674–683, 2003.

[26] Z. L. Wang and A. C. Wang, "On the origin of contact-electrification," *Materials Today*, vol. 30, pp. 34–51, 2019.

[27] S. Lin, L. Xu, A. C. Wang, and Z. L. Wang, "Quantifying electron-transfer in liquid-solid contact electrification and the formation of electric double-layer," *Nature communications*, vol. 11, no. 1, pp. 1–8, 2020.

[28] M. Machesky, D. Wesolowski, D. Palmer, M. Ridley, P. Bénézeth, S. Lvov, and M. Fedkin, "Chapter 12 - ion adsorption into the hydrothermal regime: Experimental and modeling approaches," in *Surface Complexation Modelling* (J. Lützenkirchen, ed.), vol. 11 of *Interface Science and Technology*, pp. 324–358, Elsevier, 2006.

[29] O. Bonhomme, B. Blanc, L. Joly, C. Ybert, and A.-L. Biance, "Electrokinetic transport in liquid foams," *Advances in Colloid and Interface Science*, vol. 247, pp. 477–490, 2017. Dominique Langevin Festschrift: Four Decades Opening Gates in Colloid and Interface Science.

[30] F. Booth, "Theory of electrokinetic effects," 1948.

[31] M. von Smoluchowski, "Contribution à la théorie de l'endosmose électrique et de quelques phénomènes corrélatifs," *Bull. Akad. Sci. Cracovie.*, vol. 8, pp. 182–200, 1903.

[32] N. Nuchtavorn, W. Suntornsuk, S. M. Lunte, and L. Suntornsuk, "Recent applications of microchip electrophoresis to biomedical analysis," *Journal of Pharmaceutical and Biomedical Analysis*, vol. 113, pp. 72–96, 2015. REVIEW 2015.

[33] G. Hempel, "Biomedical applications of capillary electrophoresis," vol. 41, no. 6, pp. 720–723, 2003.

[34] S. Marbach and L. Bocquet, "Osmosis, from molecular insights to large-scale applications," *Chem. Soc. Rev.*, vol. 48, pp. 3102–3144, 2019.

[35] S. Shoji, H. Sato, and R. Zengerle, "2.09 - liquid micropumps," in *Comprehensive Microsystems* (Y. B. Gianchandani, O. Tabata, and H. Zappe, eds.), pp. 301–322, Oxford: Elsevier, 2008.

[36] T. Bøg-Hansen, "Electrophoresis — affinity techniques," in *Encyclopedia of Analytical Science (Second Edition)* (P. Worsfold, A. Townshend, and C. Poole, eds.), pp. 419–425, Oxford: Elsevier, second edition ed., 2005.

[37] S. Ghosal, "Lubrication theory for electro-osmotic flow in a microfluidic channel of slowly varying cross-section and wall charge," *Journal of Fluid Mechanics*, vol. 459, p. 103, 2002.

[38] S. Bai, P. Huang, Y. Meng, and S. Wen, "Modeling and analysis of interfacial electrokinetic effects on thin film lubrication," *Tribology International*, vol. 39, no. 11, pp. 1405–1412, 2006.

[39] P. Vainshtein and C. Gutfinger, "On electroviscous effects in microchannels," *Journal of micromechanics and microengineering*, vol. 12, no. 3, p. 252, 2002.

[40] T. Van de Ven, "On the role of ion size in coagulation," *Journal of colloid and interface science*, vol. 124, no. 1, pp. 138–145, 1988.

[41] T. G. ávan de Ven *et al.*, "Electroviscous forces," *Faraday Discussions of the Chemical Society*, vol. 90, pp. 313–321, 1990.

[42] G. Stokes, "On the effect of internal friction of fluids on the motion of pendulums," *Trans. Camb. phi1. S0c*, vol. 9, no. 8, p. 251, 1850.

[43] H. Brenner, "The slow motion of a sphere through a viscous fluid towards a plane surface," *Chemical engineering science*, vol. 16, no. 3-4, pp. 242–251, 1961.

[44] A. Maali, R. Boisgard, H. Chraibi, Z. Zhang, H. Kellay, and A. Würger, "Viscoelastic

drag forces and crossover from no-slip to slip boundary conditions for flow near air-water interfaces," *Physical review letters*, vol. 118, no. 8, p. 084501, 2017.

[45] H. Zeng, Y. Tian, T. H. Anderson, M. Tirrell, and J. N. Israelachvili, "New sfa techniques for studying surface forces and thin film patterns induced by electric fields," *Langmuir*, vol. 24, no. 4, pp. 1173–1182, 2008.

[46] L. Richter, P. J. Zuk, P. Szymczak, J. Paczesny, K. M. Bak, T. Szymborski, P. Garstecki, H. A. Stone, R. Holyst, and C. Drummond, "Ions in an ac electric field: Strong long-range repulsion between oppositely charged surfaces," *Physical review letters*, vol. 125, no. 5, p. 056001, 2020.

[47] B. Cappella and G. Dietler, "Force-distance curves by atomic force microscopy," *Surface Science Reports*, vol. 34, no. 1, pp. 1–104, 1999.

[48] F. Liu, C. Zhao, F. Mugele, and D. van den Ende, "Amplitude modulation atomic force microscopy, is acoustic driving in liquid quantitatively reliable?," *Nanotechnology*, vol. 26, no. 38, p. 385703, 2015.

[49] J. Israelachvili and H. Wennerström, "Role of hydration and water structure in biological and colloidal interactions," *Nature*, vol. 379, no. 6562, pp. 219–225, 1996.

[50] R. Raiteri, M. Grattarola, and H.-J. Butt, "Measuring electrostatic double-layer forces at high surface potentials with the atomic force microscope," *The Journal of Physical Chemistry*, vol. 100, no. 41, pp. 16700–16705, 1996.

[51] J. Comtet, A. Niguès, V. Kaiser, B. Coasne, L. Bocquet, and A. Siria, "Nanoscale capillary freezing of ionic liquids confined between metallic interfaces and the role of electronic screening," *Nature materials*, vol. 16, no. 6, p. 634, 2017.

[52] R. Villey, E. Martinot, C. Cottin-Bizonne, M. Phaner-Goutorbe, L. Léger, F. Restagno, and E. Charlaix, "Effect of surface elasticity on the rheology of nanometric liquids," *Physical review letters*, vol. 111, no. 21, p. 215701, 2013.

[53] A. Steinberger, C. Cottin-Bizonne, P. Kleimann, and E. Charlaix, "Nanoscale flow on a bubble mattress: Effect of surface elasticity," *Physical review letters*, vol. 100, no. 13, p. 134501, 2008.

[54] S. Leroy, A. Steinberger, C. Cottin-Bizonne, F. Restagno, L. Léger, and E. Charlaix, "Hydrodynamic interaction between a spherical particle and an elastic surface: a gentle probe for soft thin films," *Physical review letters*, vol. 108, no. 26, p. 264501, 2012.

[55] L. Garcia, *Étude rhéologique des électrolytes confinés en appareil à forces de surfaces dynamique*. PhD thesis, Grenoble Alpes, 2016.

[56] L. Garcia, L. Jacquot, E. Charlaix, and B. Cross, "Nano-mechanics of ionic liquids at dielectric and metallic interfaces," *Faraday Discussions*, vol. 206, pp. 443–457, 2017.

[57] A. Maali, T. Cohen-Bouhacina, C. Hurth, C. Jai, R. Boisgard, and J.-P. Aimé, *Dynamic AFM in Liquids: Viscous Damping and Applications to the Study of Confined Liquids*, pp. 149–164. Berlin, Heidelberg: Springer Berlin Heidelberg, 2009.

[58] D. Andelman, "Electrostatic properties of membranes: the poisson-boltzmann theory," in *Handbook of biological physics*, vol. 1, pp. 603–642, Elsevier, 1995.

[59] D. Andelman, "Introduction to electrostatics in soft and biological matter," *Soft condensed matter physics in molecular and cell biology*, vol. 6, 2006.

[60] T. Markovich, D. Andelman, and R. Podgornik, "Charged membranes: Poisson-boltzmann theory, dlvo paradigm and beyond," *arXiv preprint arXiv:1603.09451*, 2016.

[61] C. Gray and P. J. Stiles, "Nonlinear electrostatics: the poisson–boltzmann equation," *European Journal of Physics*, vol. 39, no. 5, p. 053002, 2018.

[62] A. C. Dixon, *The elementary properties of the Elliptic functions*. 1894.

[63] I. Kovacic, L. Cveticanin, M. Zukovic, and Z. Rakaric, "Jacobi elliptic functions: a review of nonlinear oscillatory application problems," *Journal of Sound and Vibration*, vol. 380, pp. 1–36, 2016.

[64] L. Onsager, "Reciprocal relations in irreversible processes. i.," *Physical review*, vol. 37, no. 4, p. 405, 1931.

[65] L. Onsager, "Reciprocal relations in irreversible processes. ii.," *Physical review*, vol. 38, no. 12, p. 2265, 1931.

[66] R. L. Burwell Jr and R. G. Pearson, "The principle of microscopic reversibility," *The Journal of Physical Chemistry*, vol. 70, no. 1, pp. 300–302, 1966.

[67] B. D. Coleman and C. Truesdell, "On the reciprocal relations of onsager," *The Journal of Chemical Physics*, vol. 33, no. 1, pp. 28–31, 1960.

[68] S. Levine, J. R. Marriott, and K. Robinson, "Theory of electrokinetic flow in a narrow parallel-plate channel," *Journal of the Chemical Society, Faraday Transactions 2: Molecular and Chemical Physics*, vol. 71, pp. 1–11, 1975.

[69] J. L. Anderson, "Colloid transport by interfacial forces," *Annu. Rev. Fluid Mech.*, vol. 21, no. 1, pp. 61–99, 1989.

[70] D. Stein, M. Kruithof, and C. Dekker, "Surface-charge-governed ion transport in nanofluidic channels," *Physical Review Letters*, vol. 93, no. 3, p. 035901, 2004.

[71] M. Manghi, J. Palmeri, K. Yazda, F. Henn, and V. Jourdain, "Role of charge regulation and flow slip in the ionic conductance of nanopores: An analytical approach," *Physical Review E*, vol. 98, no. 1, p. 012605, 2018.

[72] D. Ben-Yaakov, D. Andelman, D. Harries, and R. Podgornik, "Beyond standard poisson–boltzmann theory: ion-specific interactions in aqueous solutions," *Journal of Physics: Condensed Matter*, vol. 21, p. 424106, sep 2009.

[73] W. A. Ducker, T. J. Senden, and R. M. Pashley, "Direct measurement of colloidal forces using an atomic force microscope," *Nature*, vol. 353, no. 6341, pp. 239–241, 1991.

[74] J. Happel and H. Brenner, *Low Reynolds number hydrodynamics: with special applications to particulate media*, vol. 1. Springer Science & Business Media, 2012.

[75] B. M. Alexander and D. C. Prieve, "A hydrodynamic technique for measurement of colloidal forces," *Langmuir*, vol. 3, no. 5, pp. 788–795, 1987.

[76] M. Abramowitz and I. A. Stegun, *Handbook of Mathematical Functions*. New York: Dover, 1964.

[77] T. Markovich, D. Andelman, and R. Podgornik, "Charge regulation: A generalized boundary condition?," *EPL (Europhysics Letters)*, vol. 113, no. 2, p. 26004, 2016.

[78] G. Trefalt, S. H. Behrens, and M. Borkovec, "Charge regulation in the electrical double layer: ion adsorption and surface interactions," *Langmuir*, vol. 32, no. 2, pp. 380–400, 2016.

[79] T. W. Healy and L. R. White, "Ionizable surface group models of aqueous interfaces," *Advances in Colloid and Interface Science*, vol. 9, no. 4, pp. 303–345, 1978.

[80] S. H. Behrens and M. Borkovec, "Electrostatic interaction of colloidal surfaces with variable charge," *The Journal of Physical Chemistry B*, vol. 103, no. 15, pp. 2918–2928, 1999.

[81] Kelly Miller, "Disjoining pressure —lectures for ap225," 2011. [Online; accessed 31-May-2022].

[82] B. Derjaguin, "Untersuchungen über die reibung und adhäsion, iv," *Kolloid-Zeitschrift*, vol. 69, no. 2, pp. 155–164, 1934.

[83] T. Markovich, D. Andelman, and R. Podgornik, "Charge regulation: A generalized boundary condition?," *Europhys. Lett.*, vol. 113, p. 26004, jan 2016.

[84] J. N. Israelachvili, *Intermolecular and surface forces*. Academic Press London, San Diego, 2nd ed. ed., 1991.

[85] A. Maali and R. Boisgard, "Precise damping and stiffness extraction in acoustic driven cantilever in liquid," *Journal of Applied Physics*, vol. 114, no. 14, p. 144302, 2013.